IEEE Access
Multidisciplinary | Rapid Review | Open Access Journal

Received 3 April 2023, accepted 25 April 2023, date of publication 16 May 2023, date of current version 9 June 2023.

Digital Object Identifier 10.1109/ACCESS.2023.3276883

RESEARCH ARTICLE

A Compact Filter and Dipole Antenna With Its Phased Array Filtenna and ADMM-BO Learning for Use-Case Analog/Hybrid Beamforming in 5G mmWave Communications

MAHDI NOURI[1], (Member, IEEE), ALIREZA JAFARIEH[1], (Student Member, IEEE), HAMID BEHROOZI[1], (Member, IEEE), NAZIH KHADDAJ MALLAT[2], (Senior Member, IEEE), AMJAD IQBAL[2,3], (Member, IEEE), MD. JALIL PIRAN[4], (Senior Member, IEEE), AND DUEHEE LEE[5], (Member, IEEE)

[1]Department of Electrical Engineering, Sharif University of Technology, Tehran 3155267188, Iran
[2]College of Engineering, Al Ain University, Al Ain, United Arab Emirates
[3]Institut National de la Recherche Scientifique (INRS-EMT), Montreal, QC H5A 1K6, Canada
[4]Department of Computer Science and Electrical Engineering, Sejong University, Seoul 05006, South Korea
[5]Department of Electrical Engineering, Konkuk University, Seoul 05029, South Korea

Corresponding author: Hamid Behroozi (behroozi@sharif.edu)

This work was supported by the Iran National Science Foundation (INSF) under Grant 98005030, and the Human Resources Program in Energy Technology of the Korea Institute of Energy Technology Evaluation and Planning (KETEP) and the Ministry of Trade, Industry & Energy (MOTIE) of the Republic of Korea (No. 20204010600220).

ABSTRACT In this article, a 5G compact millimeter-wave dipole antenna with high gain and its array filter-antenna is proposed, following a theoretical discussion is proposed. To increase the gain and focused mainbeam, the double dipole is inserted at the ground plane. The results show that the proposed antenna has an impedance band-width (IBW) of around 7.14% and 6.7 dBi gain at 28 GHz. Next, a 5G filter is proposed with 4% IBW and lower than 0.6 dB gain insertion loss. A simple phase-shifter with 2-bit structure is designed in an 8-elemens array filter-antenna with 0.35λ spacing between the two elements which uses a meander-line to reduce mutual-coupling. First, the phased-array filtenna (filter-antenna) is fabricated to meet the analog beamforming challenge. The IBWs of the array filter antenna are approximately 3.5% with a high gain of 15 dBi. Second, a novel machine learning method is proposed as an alternating direction method of multipliers and Bayesian Optimization (ADMM-BO) is used in the hybrid beamforming for such partially-connected phased-array structures. Simulation and measurement results show that the proposed antenna and its array have a high gain in analog and hybrid beamforming and acceptable data rates. The data-rates of this array reach 100 Mb/s in SNRs higher than 10 dB. The amount for 0 dB SNR is 75 Mb/s. These results also indicate that the mainbeam shift is in the range of $[-50°, 50°]$ with a gain in variations of around 1.5 dB and side lobe level (SLL) of about -10 dB at 50°.

INDEX TERMS Microstrip patched antenna, 5G communication, mmwave filter, phase shifter, phased array filter-antenna, analog and hybrid beamforming, ADMM-BO.

I. INTRODUCTION

To keep pace with the progress in telecommunications, it is essential mobile devices to have a bandwidth with more frequencies and higher data rates. The fifth-generation (5G) mobile communication system can meet these challenges. These 5G mobile networks have some extra advantages over the 4G network, like beamforming, coverage growth, better energy efficiency, and cost-saving [1], [2]. The most important use of massive multi-input multi-output (MIMO)

The associate editor coordinating the review of this manuscript and approving it for publication was Davide Comite.

This work is licensed under a Creative Commons Attribution-NonCommercial-NoDerivatives 4.0 License.
For more information, see https://creativecommons.org/licenses/by-nc-nd/4.0/

in 5G mobile systems is beamforming. It changes the direction of the antenna power for various purposes, such as null steering and direction of arrival (DOA) [3], [4]. There are several analog and digital beamforming methods; however, the active-phased array is the best to apply in analog form [3], [4]. Nevertheless, low geometrical size is more convenient for designing RF devices. Therefore, the millimeter wave (mmWave) frequencies (30-300 GHz), unlike centimeter wave (CMW) frequencies (1-30 GHz), seem to present a highly suitable solution. Due to their short wavelength, antennas that work on this spectrum have small dimensions. In the USA, the licensed frequency spectrum for 5G is 27.5-28.35 (GHz), and for the UK and Europe, this spectrum is 24.25-27.5 (GHz). The frequency spectrums 27.5-28.25 (GHz), 24.25-27.5 (GHz), 26.5-29.5 (GHz), and 24.5-29 (GHz) are licensed for Japan, China, Korea, and India, respectively. Therefore, designing an innovative low-size active array filter-antenna (filtenna) for mmWave beamforming could be a very potential goal in 5G communication systems [5].

A. RELATED WORKS

Various antennas for 5G applications have been proposed [5], [6], [7], [8], [9], [10], [11]. A dual-band planar 5G mmWave antenna is proposed in [5]. This antenna has high gain and Impedance band-width (IBW), low side lobe level (SLL), and compact size. Furthermore, theoretical discussions are included in this paper, based on the equivalent circuit model. Another dipole antenna with four modes is presented in [6]. The benefits of this antenna are the high gain in its different modes and the fact that it works in dual frequency bands. Unfortunately, the dimensions of this antenna are very large and no theoretical discussions are proposed in this work. A 1×4 planar array antenna was suggested, benefiting from several advantages such as high gain, around 11 dBi, low cost, compactness, and fan-beam [7]. The authors in [8] proposed a 5G array antenna in 28-GHz with a CMOS direct conversion transceiver for a wireless cellular mobile system. This antenna achieves a high gain (almost 13 dBi) and compact size for 5G indoor applications.

Not covering European standards is a disadvantage of this apparatus. A compact mmWave multi-layer microstrip Rotman lens is proposed in [9]. One of the applications of the Rotman lens is beamforming. This work achieves 14.5 dBi gain and provides different angles of beamspace. However, it has a thick substrate and does not cover the European licensed spectrum, either. In [10], an mmWave flexible 5G antenna for wireless applications with a wide frequency bandwidth is suggested, that covers both European and USA standards but has large dimensions. Another single antenna with an omnidirectional beam and an appropriate frequency bandwidth (27-28.5GHz) for the 5G applications is recommended in [11]. This work releases very low gain (around 2 dBi) and is not compact.

Several designs of filters are proposed in [12], [13], [14], [15], and [16]. The authors in [12] propose a dual band filter with applications on mmWave 5G. The merits of this filter are high out of band rejection and low thickness. However, this design has high insertion loss (IL) and large dimension. Another CMW filter with high out of band rejection and low IL is proposed in [13]. A disadvantage of this filter is its great thickness. A half mode substrate integrated waveguide (HMSIW) mmWave filter with high IBW, low IL, and high out of band rejection is proposed in [14]. In the above works, theoretical aspects of the filter are not discussed. The authors in [15] propose a substrate integrated waveguide (SIW) sub-6 5G filter with low IL, high out of band rejection, and support the proposal with theoretical discussion. However, this filter is very thick. A dualband mmWave 5G filter with low IL, high out of band rejection, and theoretical discussions based on an LC-equivalent circuit is proposed in [16].

The demand for high BW on the 5G frequency bands and the requirement of a large stopband on the non-desired frequencies invite us to use filters integrated with an antenna as filtenna [17], [18]. In [17], the authors propose an mmWave microstrip filter with high out of band rejection, and low IL. This filter is not compact and is thick. The antenna proposed in [17] has sufficient gain and IBW. However, the dimensions of this antenna are pretty large. In [18], an mmWave microstrip filter is proposed with high out of band rejection, very low IL, and high IBW for 5G systems. Unfortunately, this filter has large dimensions. The antenna proposed in [18] has a large IBW and high gain. The dimension of this antenna is large, too.

Analog beamforming method uses analog phase-shifters (PSs), which enforce a fixed amplitude constraint on the antenna elements. This limitation imposes analog beamforming and offers poor performance in comparison to the fully digital beamforming schemes [19], [20], [21]. In conventional fully digital beamforming, any antenna element needs one radio frequency (RF) chain which adds exponential complexity in 5G mmWave systems due to the large number of antenna elements in the array antenna [22], [23]. Hybrid beamforming divides the total complexity between the two analog and digital parts which decreases the number of RF chains while achieving appropriate data rates and beamforming gain [20], [21], [22], [23].

B. MAIN CONTRIBUTIONS

The acronyms used in this article are presented in Table 1. In this paper, the contributions can be listed as follows:

- An initial equivalent circuit for an mmWave filter is proposed. Based on this equivalent model, an initial filter is designed with a resonance frequency near 28 GHz. To achieve the desired passband and transmission zeros (TZ), the equivalent circuit is modified. Stubs are added to the filter. The effect of the design parameters on the resonance frequency is investigated. Based on this investigation a reconfigurable design is achieved. The final filter has low dimensions ($3.64 \times 6.32\ mm^2$), low insertion loss (0.6 dB), and

TABLE 1. Acronyms and definitions.

Abbreviation	Definition
ADMM-BO	Alternating direction method of multipliers-Bayesian Optimization
BW	Bandwidth
CMW	Centimeter-wave
DOA	Direction of arrival
EE	Energy efficiency
G	Gain
HFSS	High-frequency structure simulator
HMSIW	Half mode substrate integrated waveguide
HPBW	Half power beamwidth
IBW	Impedance bandwidth
IL	Insertion loss
ITU	International telecommunication union
mmWave	Millimeter-wave
MIMO	Multi input multi output
PS	Phase-shifter
SE	Spectral efficiency
SIW	Substrate integrated waveguide
SLL	Side-lobe level
WC	With-out capacitor

high out of band rejection (45 dB). The final design is fabricated on a Rogers RT/duroid 5880 substrate (ε_r = 2.2, h=0.32 mm).

- An initial equivalent circuit for an mmWave antenna is proposed. A monopole antenna based on this equivalent circuit is designed. Then, to control the resonance frequency, antenna gain, and antenna beam, a U-shaped bend slot and dipoles on the ground plane are added. The effect of one of the design variables on the antenna's operation band is investigated. The proposed antenna has a 6.5 dB maximum gain on the operation band, 5 % IBW, and more than 90 % radiation efficiency. This antenna is compared with some other state-of-the-art equivalents. The dimension of this antenna is smaller than most of them. This antenna also has a thinner substrate than most. This antenna is fabricated on a Rogers RT/duroid 5880 substrate ($\varepsilon_r = 2.2$, h=0.32 mm).
- A design 5G active phased array filter antenna is discussed. It contains the proposed filter and an 8-element antenna with an inserted two-bits phase-shifter based on delay lines, which provides a phase shift around 90°, 180°, 270°. The array has 1% IBW, a 15 dB maximum gain, and 16 dB SLL. Analog beamforming is evaluated with the proposed 5G phased array filtenna. This beamforming system can steer the beam between -50° and 50°. At the beam 50°, the peak gain drops by only 1.5 dB, but the SLL becomes -9.6 dB.
- A novel machine learning method is defined as ADMM-BO and is employed in solving the hybrid beamforming problem of the Euclidean distance error between transmitted and received signals, which contains combining and channel matrices for a proposed partially-connected two-bits phase filtenna array. To ensure low complexity, the analog beamformer matrix is optimized row-by-row by the ADMM-BO learning method. The comparative experimental results are presented in terms of spectral efficiency (SE) and BER performance, which verify the performance of the proposed hybrid beamforming method and capability of the suggested phased filtenna array.
- Complete comparisons are set out in two tables with state-of-art 5G filters, 5G antenna, and 5G array filtenna in order to investigate the main advantages of the proposed 5G collection. All electromagnetic simulations are performed by a high-frequency structure simulator (HFSS) [19].

C. ORGANIZATION OF THE PAPER

In what follows, section II describes the filter design. The proposed single antenna and theoretical discussion are presented in section III. In section IV, the phase shifter performance and proposed phased array filtenna are shown. The conclusions of the research are described in section V.

II. FILTER DESIGN

Fig. 1a) and Fig. 1b) represent the geometry of the proposed 5G filter and circuit model, respectively. The proposed filter is fabricated on a Rogers RT/duroid 5880 substrate (ε_r = 2.2, h = 0.32 mm). The Rogers RT/duroid 5880 substrate is chosen because it is one of the most popular and efficient substrates in the mmWave band. The thickness of the substrate is set to 0.32 mm to reduce the number of free parameters in the design of the filter and achieve a thin design. The red parts of Fig. 1a) show the initial design of the filter. The blue and green parts are stubs added in the second and final steps of the design, respectively. The equivalent circuit is made on the basis of LC equivalent circuits [5], [16], [25], [26], [27]. C_1 and C_2 are capacitance representing the $l_{1f} \times w_{5f}$ and $(l_{1f} - l_{10f}) \times (w_{5f} - w_{8f})$ rectangles respectively. L_1 illustrates the inductance of the L-shape feed line. The impedance of the L-shape feed line can be written as follows:

$$Z_1^f = \frac{1}{j2\pi f_c C_1} || \frac{1}{j2\pi f_c C_2} || j2\pi f_c L_1 \tag{1}$$

C_c is the coupling between the triangular and L-shape parts and is derived from [22]:

$$C_c = \frac{-(C_3 + C_4) + \sqrt{(C_3 + C_4)^2 - 4C_3C_4(1 - C_k^{-2})}}{2} \tag{2}$$

where $C_4 = C_1 || C_2$, and $C_k = \frac{1}{\sqrt{Q_1 Q_2}}$. Q_1 and Q_2 are the quality factors of Z_1^f and Z_2^f respectively. The equivalent capacitance and inductance of the triangular part of the filter are C_3 and L_3 respectively. Z_2, which represents the

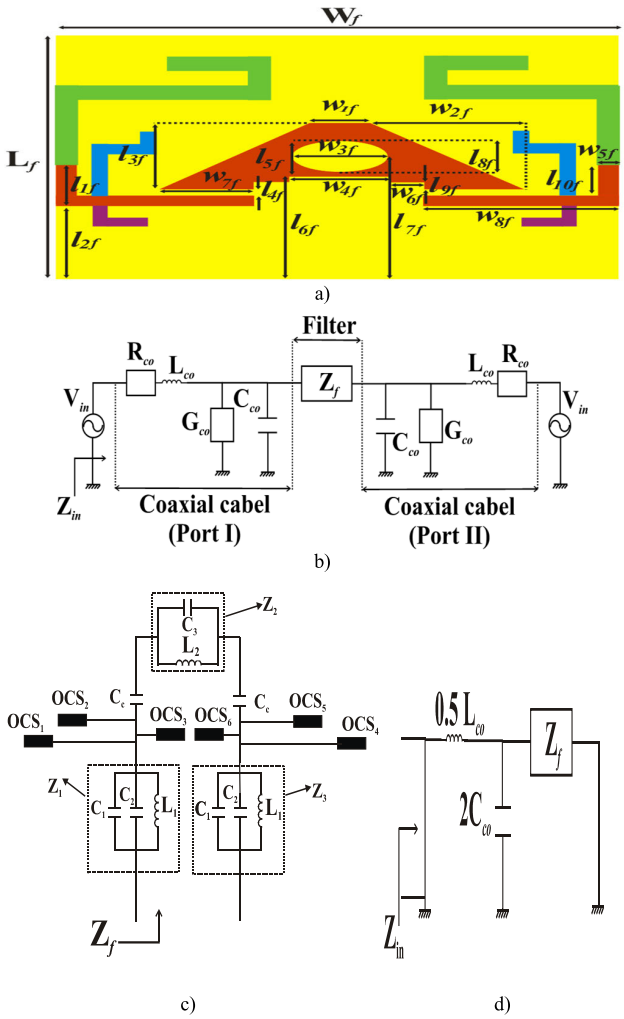

FIGURE 1. a) Geometry of the initial 5G mmWave triangular filter, red, green, and blue parts are on the onboard plane and the yellow part is the substrate; b) The equivalent circuit of the proposed filter with the SMA model; c) The equivalent circuit of Z_f.; d) The simplified circuit of the proposed circuit on b).

impedance of the triangular part, can be defined as follows:

$$Z_2^f = \frac{1}{j2\pi f_c C_3} || j2\pi f_c L_3 \tag{3}$$

The input impedance of the filter is calculated as follows:

$$Z_f = 2Z_1^f + Z_2^f + \frac{2}{j2\pi f_c C_c} \tag{4}$$

C_{co} and L_{co} on Fig. 1b) represent capacitance per unit length and inductance per unit of length of coaxial cable, respectively. R_{co} and G_{co} are resistance per unit length and conductance of the dielectric per unit length of coaxial cable. For a lossless cable, we consume $R_{co} = G_{co} = 0$. The SMA connector model is RF 132134-10. In order to calculate Z_{in} from the initial design, a simplified circuit is proposed in Fig. 1d) with respect to the symmetric design of Fig. 1b), and low loss of coaxial cable ($R_{co} = G_{co} = 0$), and then, to achieve Z_{in}, voltage sources are turned to short circuit. The

TABLE 2. The equivalent LC-circuit components of the proposed 5G filter.

C_1	C_2	C_3	L_1	L_2	R	C_{co}	L_{co}	C_c
0.098 pF	0.049 pF	0.61 pF	2 nH	3.2 nH	50 Ω	150 pF/m	250 nH/m	0.6 pF

Input impedance of the initial design is calculated from:

$$Z_{in} = Z_f || \frac{0.5}{j2\pi f_c C_{co}} || 0.5\,(j2\pi f_c L_{co}) \tag{5}$$

The resonance frequency accrues when Z_{in} becomes zero. Fig. 2a) represents the S-parameter of an equivalent circuit in the initial design for different C_3 values, while others are constant. It is obvious from this result, that changing the C3 value can significantly affect the resonance frequency. In Fig. 1a), to achieve a suitable value for C3 the ellipse part and triangle parts (l3f, w2f) are subtracted from the rectangle part (l3f, 2w2f+w1f). By changing the size of these parts, C3 can be tuned. Note that, L_2 is dependent on C_3 and changing the value of C_3,changes L_2 also.

L-shape feed lines have a 50 Ω impedance match which makes this filter suitable for 5G applications such as filtennas. This initial design has 0.4 dB attenuation on the pass-band. However, the out of band rejection of the initial filter (shown in red in Fig. 1a)) is low. In order to increase the rejection on the lower cut-off frequency, two blue stubs (shown in Fig. 1c) as OCS3, OCS6) are added to Fig. 1a). These stubs create high rejection in the 20 GHz-25GHz band. But adding these stubs has the effect on the main resonance of shifting it. To omit this shift in main resonance frequency purple stubs (shown in Fig. 1c) as OCS1, OCS4) are added. Finally, to increase the rejection at a higher cut-off frequency, green stubs (shown in Fig. 1c) as OCS2, OCS5) are added to the filter design. Fig. 2b) represents the S-parameter of the circuit equivalent model of the final design. The responses of the equivalent circuits are made possible by means of ADS V.19 software. The optimized values of the equivalent LC-circuit components are given in Table 2.

Fig. 2c) and Fig. 2d) show the simulated S-parameter of the filter for the initial, second, and final designs. From Fig. 2c), adding blue stubs caused small resonance to be omitted on the 21 GHz frequency, and consequent attenuation on this frequency from −5 dB to −50 dB. Adding green stubs, is caused by rising attenuation on the 30 GHz frequency from −5 dB to −40 dB. Fig. 2e) compares the theoretical and simulation results. They are found to differ in the location of the nulls and bandwidth of the filter. The main reason for this difference is the loss of stubs, microstrip lines, and dielectric. The equivalent circuits help us to understand the effect of the design parameters and avoid test-trial designs. However, this method cannot supply the true bandwidth of the filter which lead us to use electromagnetic simulators like Ansoft-HFSS.

Fig. 3a) and Fig. 3b) propose the real and imaginary parts of the input impedance of the filter, respectively. It can be understood from this results that the initial design has a resonance in 21 GHz but the blue stubs change it to

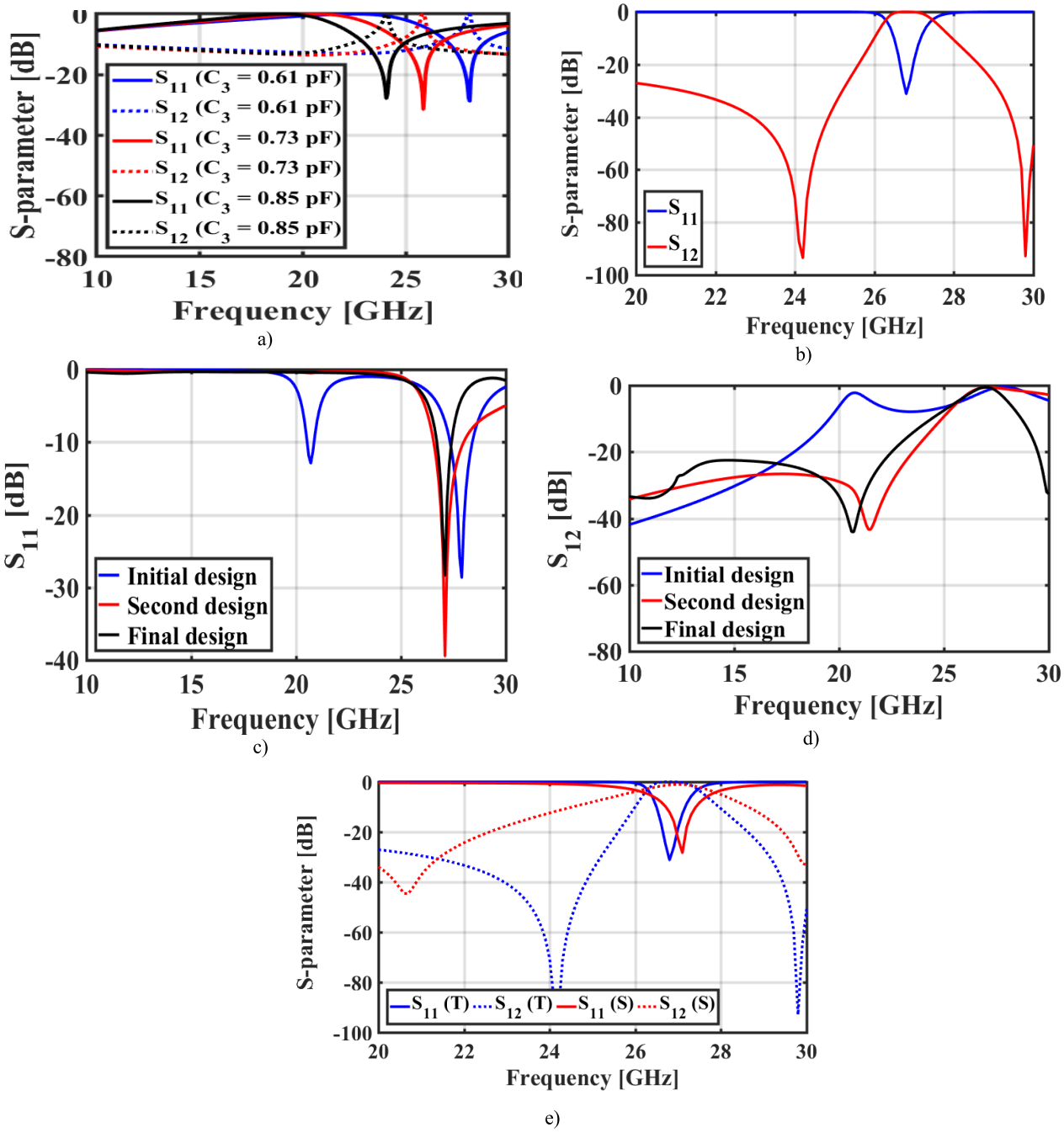

FIGURE 2. a) The S-parameter of the equivalent circuit of the initial filter for different C_3 values. b) The S-parameter of the equivalent final design of the 5G filter. c) The S_{11} of the proposed 5G filter. d) The S_{12} of the proposed 5G filter. e) Comparison between theoretical results (T) and simulation results (S).

anti-resonance (a zero imaginary part and a very big real part) in 23-25 GHz band. The green stubs provide the condition to create zero transmission between frequencies of 30 and 31 GHz frequency.

We tried to trap the current on this stub in this frequency band, a point which will be further discussed in connection with Fig. 6c). With respect to 3GPP SRIT proponent (Doc. 5D/1216-E) which is approved by International Telecommunication Union (ITU) in IMT2020, a determined BW for each user can be selected from 50, 100, 200, and 400 MHz in mmWave bands. In the case of carrier aggregation, 400 and 800 MHz are assigned to each user at 28 GHz carrier frequency [2]. With respect to the ITU specifications, this filter should have a great bandwidth of approximately 0.5 GHz. Hence, the width of the resonator microstrip and gap overlap part should be reduced. It makes a wider bandwidth,

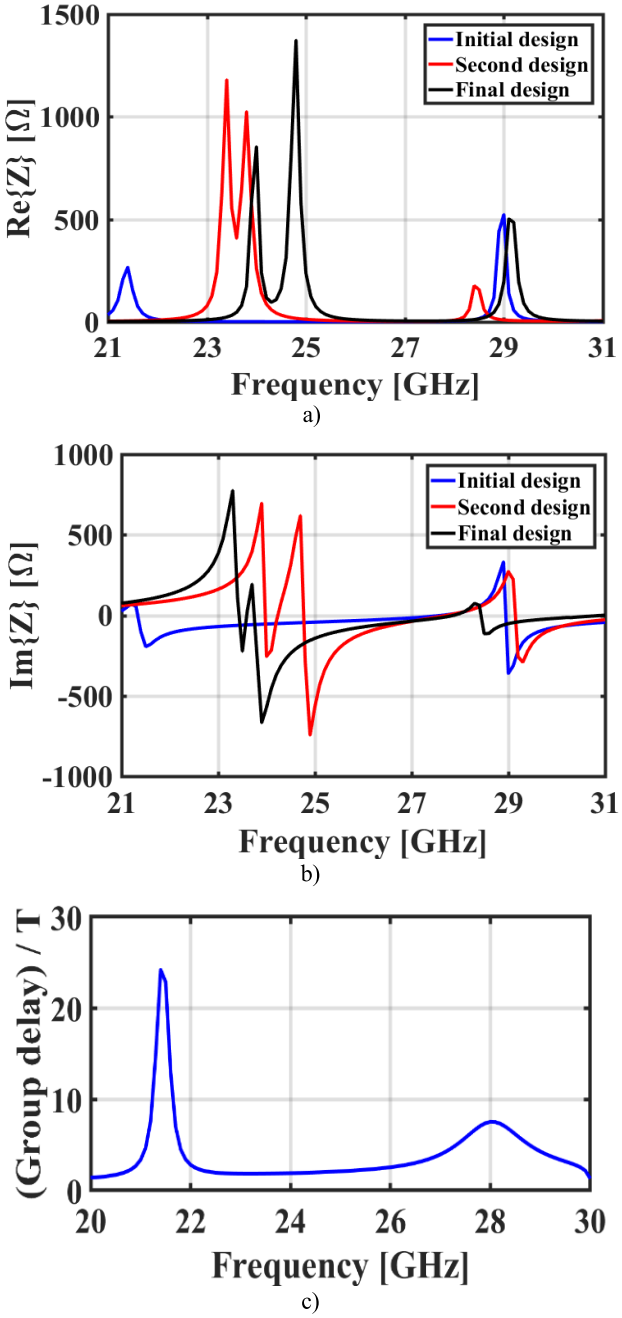

FIGURE 3. Impedance and group delay of the filter for three designs. a) real part. b) Imaginary part. c) The simulated group delay over the period (T) of the proposed filter versus frequency.

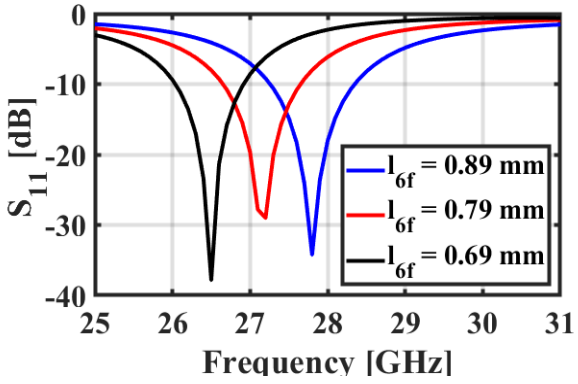

FIGURE 4. S_{11} of the proposed 5G filter for different l_6 values.

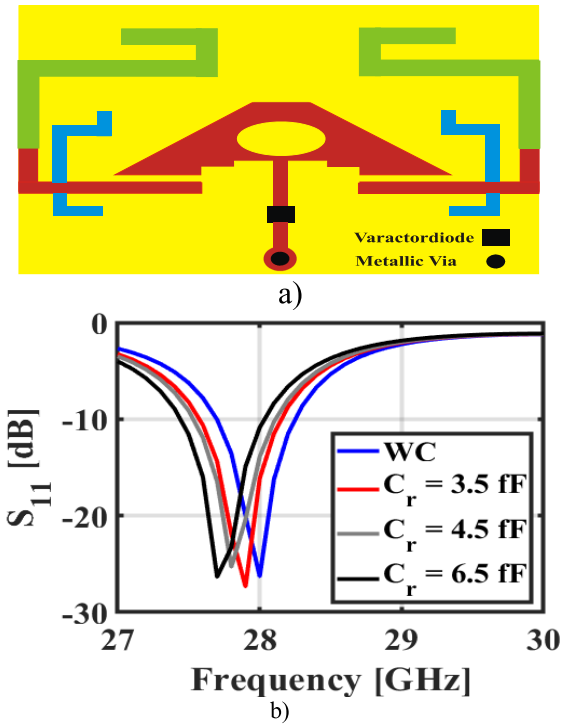

FIGURE 5. a) Proposed filter with varactor diode, b) The S_{11} of the proposed 5G filter for different C_r values. WC is the abbreviation for 'without capacitor'.

but at the same time causes lower stopband suppression. The final structure should have low L_1 and C_3 in order to secure wider bandwidth and resonance at 28 GHz. The optimized value of the filter design parameters is proposed in Table 3, and the dimensions of the stubs are as follows: $OCS_1 = OCS_4 = 0.16 \times 0.86\ mm^2$, $OCS_3 = OCS_6 = 0.16 \times 2.35\ mm^2$, and $OCS_2 = OCS_5 = 0.26 \times 5.65\ mm^2$. This filter has a low profile ($0.34\lambda_o \times 0.59\lambda_o$) and 1% BW on the 28 GHz operating frequency, which is consonant with the ITU standards. In the initial filter (Fig. 2a)), the out of band attenuation is lower than 15 dB, and in the final design it is -50 dB and -40 dB for the lower and higher cut-off frequencies, respectively. The group delay over the period (T) of the proposed filter versus frequency is illustrated in Fig. 3 c). Where, T = 1/f, is the period of signal in each frequency. In the 28 GHz frequency, the group delay is 7.5 times T.

The BW of the equivalent circuit is bigger than the BW of the 5G mmWave filter, and the 3 dB BW of the equivalent circuit is smaller than the proposed 5G mmWave filter; this is due to assuming low loss microstrip lines on the equivalent circuit model. Table 4 compares the proposed filter with some other filters. The proposed filter has smaller dimensions than [12], [17], and [18]. Our design is not as

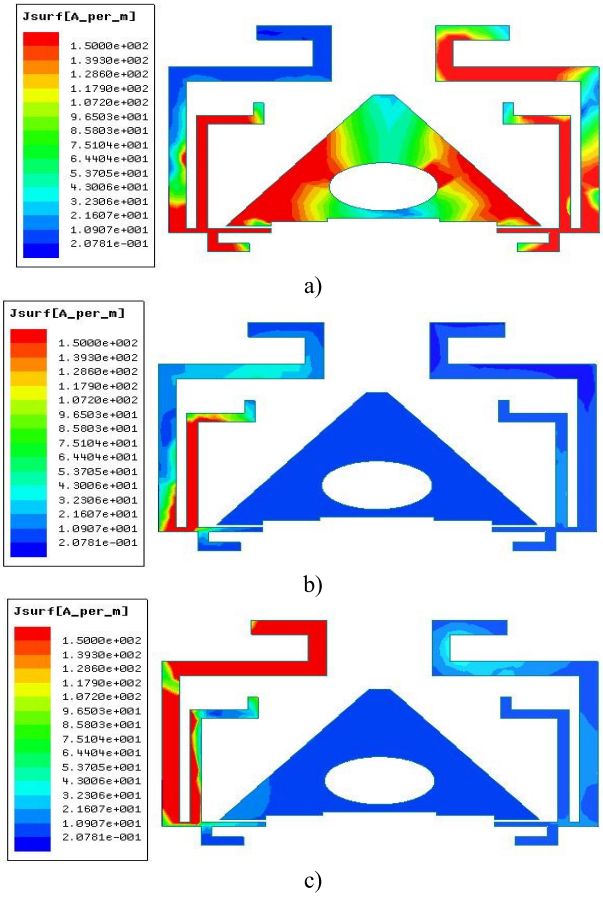

FIGURE 6. Surface current for the proposed 5G mmWave filter in various frequencies, a) 28 GHz, b) 21 GHz, c) 30 GHz.

TABLE 3. Design parameters of the proposed 5G filter.

Param.	Val.(mm)	Param.	Val.(mm)	Param.	Val.(mm)
W_f	6.38	L_f	3.72	w_{7f}	0.66
w_{1f}	0.31	l_{1f}	0.82	w_{8f}	1.51
w_{2f}	2.18	l_{2f}	0.64	l_{7f}	1.45
w_{3f}	1.61	l_{3f}	2.32	l_{8f}	0.85
w_{4f}	1.67	l_{4f}	0.04	l_{9f}	0.06
w_{5f}	0.26	l_{5f}	1.12	l_{10f}	0.74
w_{6f}	0.26	l_{6f}	0.89	-	-

thick as that proposed in [17]. The IL of the proposed filter is lower than those presented in [12], [14], [16], and [17]. The rejection of our filter is higher than all the compared designs. With respect to theoretical discussions, in order to change the passband of the filter, the value of C_3 should be changed. In order to change this value, there are two kinds of solution:

A. DYNAMIC RESONANCE FREQUENCY

The dimension of the filter should be changed. Fig. 4 shows the impact of l_{6f} on the S-parameter of the filter. Decreasing this value increases C_3 and thereby decreases the resonance frequency. However, it is not practical to change the filter dimension in a 5G device.

B. RECONFIGURABLE FILTER WITH A PARALLEL VARACTOR DIODE

As an alternative solution, a parallel capacitor, C_r, is added to the filter as Fig. 5a). In fact, this capacitor is parallel with C_3, and will lead to an increase in the value of the capacitance part of Z_2. Fig. 5b) depicts the effect of C_r on the S-parameter of the filter. Changing this value can change the resonance frequency with 100 MHz resolution. However, this reconfigurable filter is not fabricated in this paper. It only mentioned as an alternative solution for those who need this filter in another operation frequency. The simulated surface current distribution of the filter on CW mode can be seen in Fig. 6, which shows the filtering performance for the 28 GHz, 21 GHz, and 30 GHz frequencies. It can be seen that the surface current of the filter is transmitted from one port to another on the 28 GHz frequency.

However, the surface current is trapped on the OCS_3 and $OCS_2$for the 21 GHz and 30 GHz frequencies, respectively. In the 28 GHz frequency, most parts of the filter are red (which shows the highest simulated current surface). This shows how current flows from one port to the other. But in Fig. 6b) only the OC3 stub becomes red and other parts of the filter are dark blue (which shows the lowest surface current). Similarly, in Fig. 6c) only the OC2 stub becomes red. This shows that OC3 and OC2 stubs have transformed the open circuit into a short circuit at 21 GHz and 30 GHz, respectively., and, therefore, that most of the current flows in these stubs. This transformation in these frequencies looks like a trap that prevents the current from flowing between the ports.

III. MATH SINGLE ELEMENT STRUCTURE

The initial frontal geometry of the monopole antenna in Fig. 7a), is assumed for this research. This structure is inspired by the monopole antennas proposed in [28], [29], [30], and [31]. The substrate of these monopole antennas is changed so that loss on the mmWave band is low. A monopole antenna is fabricated on a Rogers RT/duroid 5880 substrate with a thickness of $h = 0.32$ mm. The size of the monopole antenna is reduced in comparison to those in [28], [29], [30], and [31], in order to increase the resonance frequency. This monopole is divided into 3 microstrip lines as depicted in Fig. 7a). The monopole antenna is tuned to have a resonance frequency on 45 GHz and the resonance frequency of the monopole antenna is decreased with a U-shaped slot at the front and two directors on the ground plane to achieve a resonance frequency on 28 GHz. This leads to a low-dimensional

TABLE 4. Comparison table of the proposed 5G filter and other recent filters.

Design	f_o (GHz)	Dimension	Relative area	IBW (%)	mmWave	CM W	5G	Insertion Loss (dB)	Technology	Rejection (dB)	h (mm)
[12]	14 &28	$0.46\lambda_o \times 1.4\lambda_o$	3.2	1	✓	✓	✓	1.9 & 4.7	microstrip	40	0.127
[13]	3.3 & 5.8	-	-	-	×	✓	×	0.2	HMSIW	40	1.575
[14]	23	$0.5\lambda_o \times 0.09\lambda_o$	0.22	30	✓	×	✓	< 1	HMSIW	20	0.25
[15]	3.5	-	-	-	×	✓	✓	0.2	SIW	20	1.575
[16]	28 & 38.5	$0.27\lambda_o \times 0.31\lambda_o$	0.47	2.1 1.3	✓	×	✓	1 0.2	microstrip	30	0.16
[17]	30	$0.34\lambda_o \times 1.17\lambda_o$	1.98	46	✓	×	✓	1	microstrip	30	0.762
[18]	30	$0.88\lambda_o \times 0.45\lambda_o$	1.68	30	✓	×	✓	< 0.1	microstrip	35	0.25
Proposed filter	28	$0.34\lambda_o \times 0.59\lambda_o$	1	1	✓	×	✓	0.6	microstrip	45	0.32

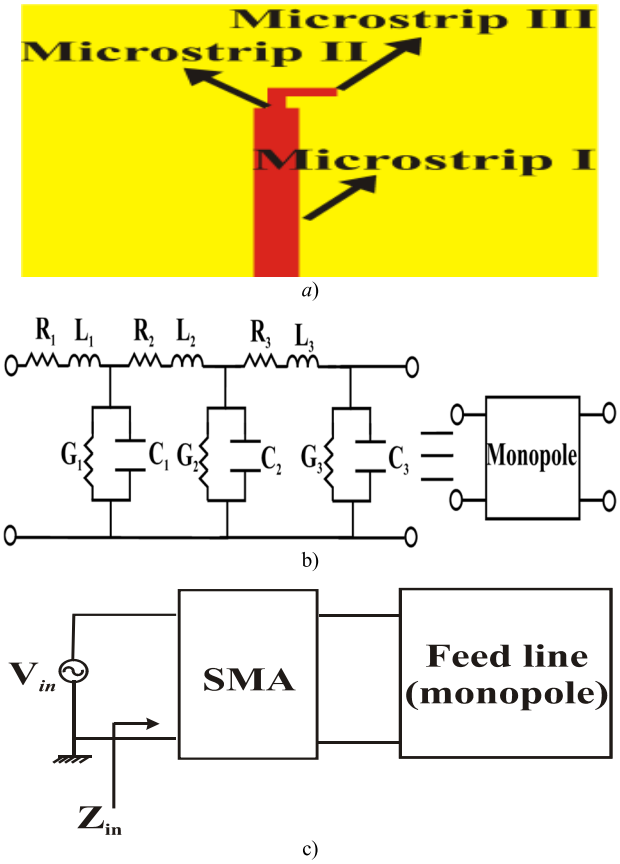

FIGURE 7. a) Monopole antenna structure, b) monopole antenna equivalent circuit. c) monopole antenna and SMA connector equivalent circuit.

resonance frequency on the desired band. In addition, these directors help to provide high gain and a directive beam, since the proposed antennas in [28], [29], [30], and [31] have low gain and an omnidirectional pattern. The theoretical discussions of the proposed antenna are given by equivalent circuits [5], [25], [26], and [27]. Each line can be modeled by a serial inductance, resistance, and a shunt conductance with a shunt capacitance. Z_0 investigates the characteristic impedance of the microstrip line. In a situation where $R \ll 2\pi f_c L$, and $G \ll 2\pi f_c C$, the microstrip line is considered a low loss line. In high frequencies, these conditions are fulfilled easily [25], [26]. Capacitance per unit of length of a microstrip line with a width of w on a substrate with ε_r permittivity and thickness of h is defined as follows [27]:

$$\mathbf{C} = \begin{cases} \frac{\varepsilon_e}{60c \times \ln\left(\frac{8h}{w} + \frac{w}{4h}\right)} & \frac{w}{h} \le 1 \\ \varepsilon_0 \varepsilon_e \left\{ \frac{w}{h} + 2.42 - 0.44\frac{h}{w} + \left(1 - \frac{h}{w}\right)^6 \right\} & \frac{w}{h} \ge 1 \end{cases} \quad (6)$$

where ε_e is the effective impedance of the substrate and calculated as $\varepsilon_e = \frac{\varepsilon_r+1}{2} + \frac{\varepsilon_r-1}{2}\left(1 + \frac{12.h}{w}\right)$. ε_r and ε_0 stand as the relative permittivity of the substrate and free air, respectively. c shows the speed of light and ε_0 equals to $\frac{10^{-9}}{36\pi}$ [26]. The inductance of the microstrip line is defined as follows:

$$L = \frac{1}{j2\pi f_c}\left(Z_0^2 (G + j2\pi f_c C) - R\right) \quad (7)$$

Fig. 7 b) shows the equivalent circuit of the monopole antenna. The final calculated input impedance of the monopole antenna based on the equivalent circuit in Figure 7 c) can be written as:

$$Z_{in}^{mono} = \left(\left(\left(\left(\frac{1}{j2\pi f_c C_3} + j2\pi f_c L_3\right) \| \frac{1}{j2\pi f_c C_2}\right) + j2\pi f_c L_2\right) \| \frac{1}{j2\pi f_c C_1}\right) + j2\pi f_c L_1 \quad (8)$$

TABLE 5. Optimized parameters of equivalent circuits.

C_1	C_2	C_3	C_4	C_5	C_6	L_1
1.4pF	0.5pF	0.04pF	0.01pF	0.38pF	0.24pF	3.4nH
L_2	L_3	L_4	L_5	L_6	L_7	L_8
1.32nH	0.1nH	0.03nH	0.04nH	0.1nH	0.94nH	0.31nH
C_{co}	L_{co}	C_{c1}	C_{c2}	-	-	-
144 pF/m	177 nH/m	0.2 pF	0.01 pF	-	-	-

$$Z_{in} = (Z_{in}^{mono} || \frac{1}{j2\pi f_c C_{co}}) + j2\pi f_c L_{co} \tag{9}$$

Resonance frequency accrues when the imaginary part of Z_{in} ges down to zero. The reflection coefficient is defined as $S_{11} = \frac{Z_{in}-Z_0}{Z_{in}+Z_0}$. The calculated S11 of the monopole is given in Fig. 8e), based on the optimized parameter of the equivalent given in Table 5. In the next step, the dimensions of the feedline are the same as the proposed monopole antenna. However, the size of the dipole and the directors should be optimized. Fig. 8a) and Fig. 8b) shows the geometry of the proposed U-shaped bend antenna with its equivalent circuit. The equivalent circuit of the directors and the dipole is depicted in Fig. 8c) and Fig. 8d), respectively. These models are designed according to the method proposed in [27]. It can be seen C4, L4, and L5 show the capacitance and inductance of the U-shaped radiator. L6 indicates the induced inductance of the U-shaped slots. The input impedance of the equivalent circuit for the dipole antenna that is shown in Fig. 8d), is defined as follows:

$$\begin{cases} Z_1 = \frac{1}{j2\pi f_c C_6} || j2\pi f_c L_8 \\ Z_2 = \frac{1}{j2\pi f_c C_5} || j2\pi f_c L_7 \\ Z_3 = \frac{1}{j2\pi f_c C_4} || j2\pi f_c L_4 || j2\pi f_c L_5 || j2\pi f_c L_6 \\ Z_4 = \frac{1}{j2\pi f_c C_3} || ((Z_1 + C_{c1}) || Z_2 + C_{c2}) || Z_3 \end{cases} \tag{10}$$

where C_{c1} and C_{c2}show the coupling between the first and second director, and the coupling between the first director and U-shape radiator, respectively. These parameters derived from (2). L_7 and C_5, and L_8 and C_6, are the inductance and capacitance of the directors, respectively. Two parameters l_7, and l_8 on Fig. 8a), should usually be smaller than $0.5\lambda_0$, and $w_7 - w_8$ should be smaller or equal to $0.05\lambda_0$ [32]. $\lambda_0$is the wavelength of the operating frequency

$$Z_5 = \left(\frac{1}{j2\pi f_c C_1} || \left(\left(\frac{1}{j2\pi f_c C_2} || (Z_4 + j2\pi f_c L_3)\right) + j2\pi f_c L_2\right)\right) + j2\pi f_c L_1 \tag{11}$$

$$Z_{in} = (Z_5 || \frac{1}{j2\pi f_c C_{co}}) + j2\pi f_c L_{co} \tag{12}$$

Resonance frequency accrues when the imaginary part of Z_{in} drops to zero. The optimized values of the circuit parameters given in Table 5 are o operate at 28 GHz as the resonance frequency. The dimension of the U-shape radiator and directors are achieved by means of (6) and (7). This antenna has

TABLE 6. Structural parameters of proposed 5G array filtenna.

Param.	Val.(mm)	Param.	Val.(mm)	Param.	Val.(mm)
W	33	L	19.2	w_{16}	2.1
W_1	7.15	L_1	6.75	w_{17}	0.5
w_2	0.55	l_2	4.15	w_{18}	0.55
w_3	0.35	l_3	0.2	w_{19}	0.5
w_4	0.15	l_4	0.8	w_{20}	15.5
w_5	0.5	l_5	0.15	w_{21}	4
w_6	0.45	l_6	0.9	w_{22}	3.75
w_7	0.1	l_7	0.35	w_s	0.2
w_8	0.05	l_8	0.1	l_{16}	14
w_9	0.2	l_9	4.25	l_{17}	5.2
w_{10}	0.7	l_{10}	1.4	l_{18}	1.2
w_{11}	1.25	l_{11}	0.2	l_{19}	1
w_{12}	2.6	l_{12}	0.45	l_{20}	0.2
w_{13}	1.2	l_{13}	0.25	l_{21}	0.58
w_{14}	0.55	l_{14}	0.6	l_{22}	11.65
w_{15}	1	l_{15}	0.1	l_s	0.8

compact dimensions (48.26 mm^2), high gain, and appropriate frequency bandwidths. The substrate of the antenna is a Rogers RT/Duroid TM 5880 ($\varepsilon_r = 2.2$, and $\tan\delta = 0.0009$, $h = 0.32\ mm$). The optimized parameters of the proposed 5G antenna are given in Table 6. Figure 9a) shows the return loss of the single antenna element for different $l_7$values. The parameter l_7 can tune the resonance frequency without BW change. Thus, by increasing the parameter l_7 different 5G-band spectrums can be covered [27], [28]. The BW of the antenna is 1.5 GHz which complies with the ITU standards. Figure 9b) illustrates the simulation and measurement radiation efficiency results of the proposed antenna. The proposed antenna displays high and stable efficiency on the operating band. The maximum simulated efficiency on the rating band reaches 96.7% at 27 GHz. The measurement value is not very different from the simulation. The maximum measured radiation efficiency is 94 % in 28 GHz. The surface current distribution of the antenna is proposed in Figure 9c) and Figure 9d). The mismatch of the measurement and simulation results is the result of the solder which connects the SMA-connector and the antenna or filtenna. This solder can be modeled as a parasitic capacitor (PC) with the capacitance of C_{in}. For example, for the proposed antenna, input impedance is rewritten as follows:

$$Z_{in}^{new} = (\frac{1}{2\pi f_c C_{in}} || Z_{in}^{old}) \tag{13}$$

where Z_{in}^{old} is the input impedance calculated on equation (12). This PC has an effect on resonance frequency, BW, and Gain. A fabricated model of the 5G proposed design is displayed in Fig. 10. The SMA connector model is RF 132134-10 and has the same SMA connector as is used for the 5G mmWave filter (loss of frequency 28 GHz is compensated by higher input power). Fig. 11 indicates the simulation

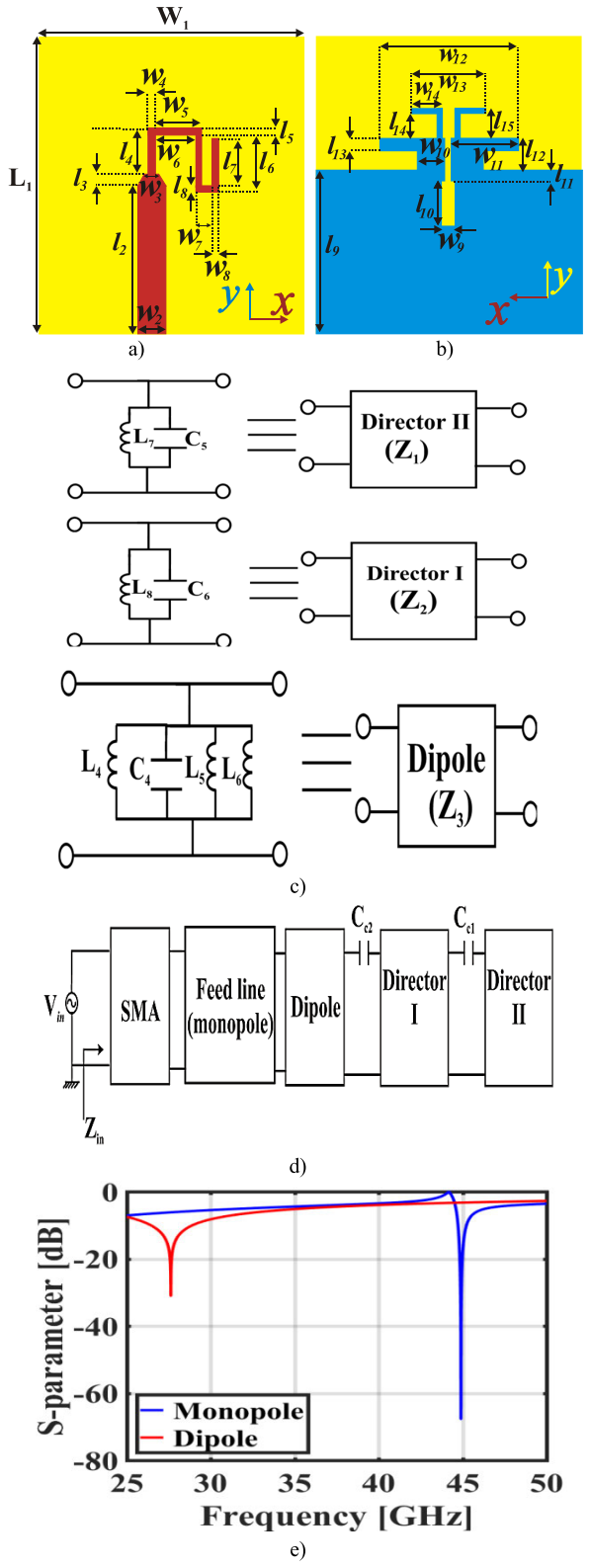

FIGURE 8. The geometry of the proposed U-shaped antenna: a) front, b) back, c) the equivalent circuit of the directors, and the equivalent circuit of the dipoles, d) the equivalent circuit of the antenna, and e) S_{11} of the equivalent circuit.

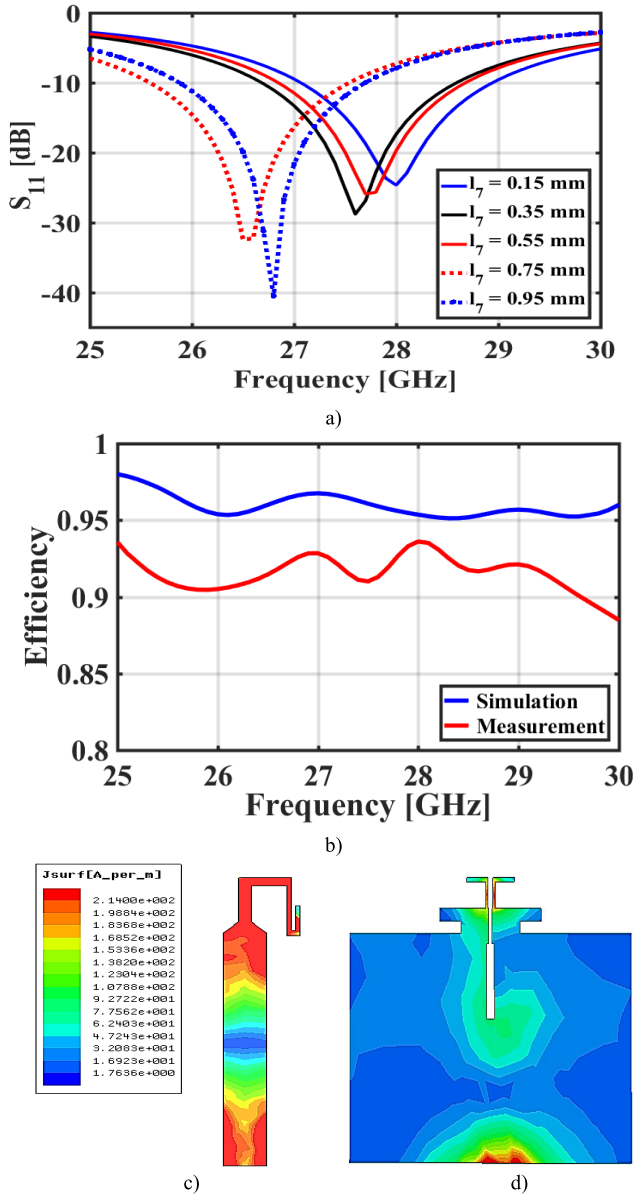

FIGURE 9. a) S-parameter of the proposed antenna for different values of l_7, b) Radiation efficiency of the simulation and measurement results, c) Antenna surface current distribution of onboard, d) Antenna surface current distribution of the ground plane.

and measurement S11 and Gain for l7 = 0.45 mm. Both simulated and measured outcomes show that the proposed antenna has sufficient bandwidth (about 1.5 GHz) to cover the 27-28.5 GHz frequency spectrum, and the consonance with the ITU standards is high enough for 5G applications. Furthermore, the maximum gain of the antenna is around 6.5 dBi for the 28 GHz frequency. Fig. 12 shows the measured and simulated E-plane and H-plane, and, as can be seen, the measured results agree with the simulation ones. The antenna pattern shows the half-power bandwidth (HPBW) of 60° for both the E- and H-planes.

IV. FILTENNA ARRAY WITH USE-CASES

To test the analog and hybrid beamforming methods, a 2-bit phase shifter is proposed. The proposed mmWave

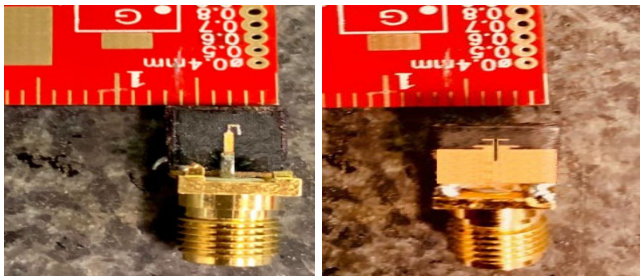

FIGURE 10. The geometry of the fabricated proposed 5G antenna with SMA connector: a) front b) back.

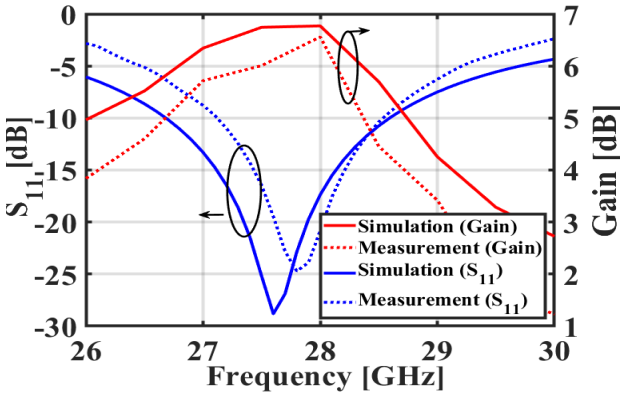

FIGURE 11. The simulation and measurement outcomes of the single antenna element: S_{11} and gain values.

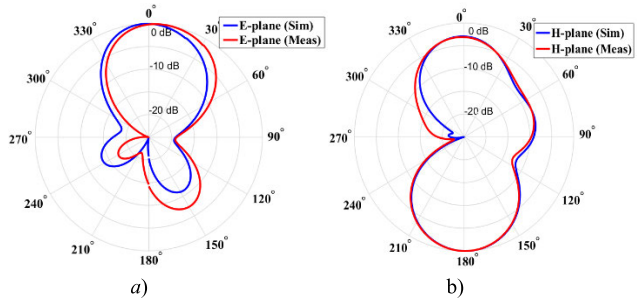

FIGURE 12. Radiation patterns of the simulation and measurement results: a) E-plane, b) H-plane.

phase shifter can provide phase shifts around 90°, 180°, and 270°. The optimized parameters of the proposed array filtenna are given in Table 6. The fabricated phase shifter on an 8-element linear array is shown in Fig. 13. The design of this phase shifter is based on the delay lines, and the SMA connector model is 52-10-TGX, which is suitable for arrays. However, this SMA connector is used for lower frequencies (up to 26.5 GHz), its loss being calculated on 28 GHz and it compensates for the transmitted power at source. If the phase of each element current changes, the amplitude remains constant.

Moreover, Fig. 13 shows the array filtenna with total dimensions of 33 × 19.2 mm^2; it is composed of

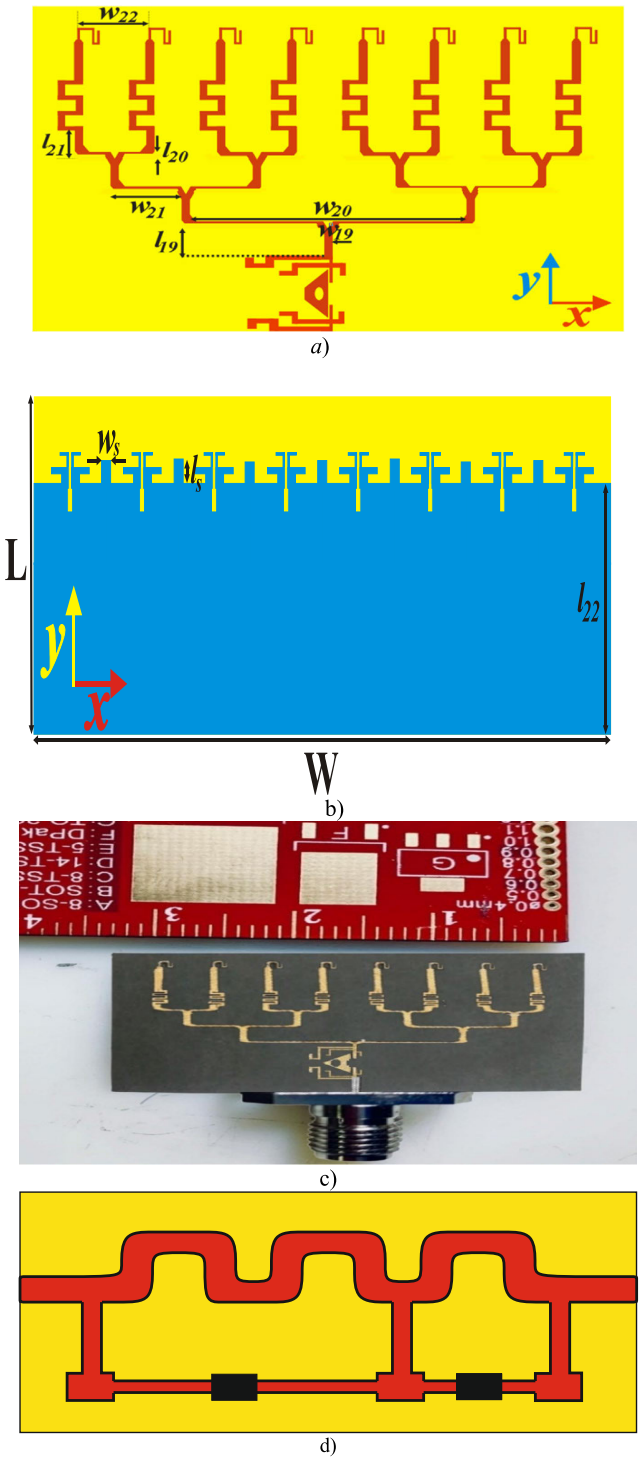

FIGURE 13. The geometry of the array filtenna: a) front view, b) back view, c) prototype of the beamforming array filtenna, d) geometry of the 2-bits phase shifter.

8 phase-shifters and 8 antenna elements. This array antenna is designed to allow analog beamforming. The proposed filter is added to the first transition line, and leads to strong suppression on the non-desired bands. Omitting non-desired signals on non-desired band in turn helps to reduce the

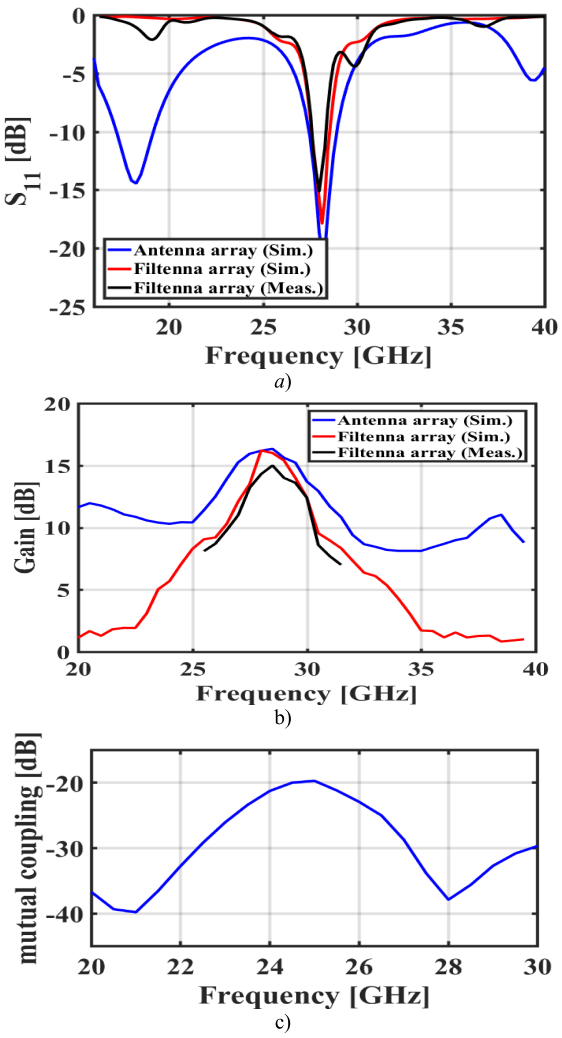

FIGURE 14. a) S_{11} performance of the 5G array filtenna in simulation and actual measurement, b) Maximum gain of the array filtenna beamforming in the simulation and measurement results. c) Simulated mutual coupling of the proposed filtenna array.

complexity of further operations such as noise-cancellation, and interference-lighting, while only a passive filter is used for all of these operations, and reducing both complexity and cost.

The maximum gain of this array is 13 dBi at angle 50° beam steering. Planted slots are placed among dipoles on the back of the array to decrease the coupling between the array elements. The directors applied on the ground plane provide a high and narrow gain. Array elements are spaced in 0.35λ. This amount was chosen to increase gain and reduce the size of the array. Furthermore, as shown in Fig. 13b) $l_s \times w_s$ stubs are added on the ground plane to reduce mutual coupling. The simulated return loss of the array antenna and array filtenna with the measured return loss of the array filtenna is presented in Fig. 14a). Going by these results, the bandwidth of the array filtenna is around 0.5 GHz, which is sufficient with respect to the ITU standards. Fig. 14b) shows the simulated and measured gain of the array filtenna and array antenna, which is almost 15 dBi at 28.5 GHz.

The surface currents of the proposed 5G array filtenna are plotted at different frequencies, namely, 28, 30, and 36 GHz in Figure 15. It can be seen that the transferred current to the array antenna is decreased by the stopband suppression in the proposed filter. Table 7 compares the proposed antenna and some other antennas. The proposed antenna has smaller dimensions than those in all the papers, except [34], [36], and [42]. The proposed antenna is not as thick as the most often compared designs, except for [10] and [18]. The realized gain of the antenna is higher than those described in [17], [34], and [35]. The radiation efficiency of this antenna is higher than those proposed in [5], [10], and [42]. Only in [7], [17], [34], and [35], and our paper was an array proposed. The array gain of the present proposed array antenna is higher than that shown in any other paper.

The filtering effect of the proposed filter in the filtenna-array is visible in Fig. 14 a). Where, two resonances of the array, 18 GHz and 30 GHz, are omitted by the filter. In addition, the filtering effect of the proposed filter is observable in Fig. 14 b). Where in the stop band of the proposed filter the realized gain of the proposed filtenna array is much less than the array (without filter). Fig.14 c) shows the mutual coupling of the proposed filtenna-array.

The filtenna array has a mutual coupling of less than 20 dB in the 20-30 GHz frequency band. Fig. 15 illustrates the surface current distribution of the proposed filtenna-array for in-band and out-of-band frequencies. 28 GHz frequency is in the pass-band of the proposed filter and 30 GHz and 26 GHz frequencies are in the rejection band of the filter. So as demonstrated in Fig. 15 the current distribution of the filtenna-array elements in 28 GHz frequency is much higher than 26 GHz, and 30 GHz. This demonstrates the filtering effect of the proposed filter in the filtenna-array.

V. USE-CASES: ANALOG AND HYBRID BEAMFORMING

A. ANALOG BEAMFORMING

Fig. 16a) exhibits the measured results of the beam-steering patterns from different angles. In analog beamforming, the gain patterns are nearly constant in a range of [-50°, 50°] with variations around 1.5 dB using only an 8-element phased array filtenna. In Fig. 16b), the beamforming performance of the proposed phase array filtenna in the terms of SLL and peak gain is displayed in graphic form. It can be seen that at beam 50° the peak gain drops only 1.5 dB, but the SLL becomes − 9.6 dBi. These experimental results show that the proposed 5G phase array filtenna can be applied to upcoming communication systems.

B. HYBRID BEAMFORMING

To support ahigh data-rate for many users in the 5G base station, it is necessary to employ beamforming, but this increases SE. However, digital beamforming is a very challenging solution for massive MIMO mmWave communications due to its

TABLE 7. Comparison table of the proposed antenna and other mmWave antennas.

Design	f_c (GHz)	IBW (%)	G (dBi)	Radiation Efficiency (%)	Dimension ($\times \lambda_c^2$)	Relative Dimension	HPBW	Array	Phased array	Beamforming angel	Array IBW (%)	Array G (dBi)	Array SLL (-dB)	Array HPBW	h (mm)
[5]	28 38	9 7.8	7.3	>80	1.7×1.6 $f_c = 28\ GHz$	6.5	$50^\circ, 30^\circ$ $90^\circ, 40^\circ$	×	×	-	-	-	-	-	0.8
[7]	28	47	8.9	-	1.87×2.1	9.4	$60^\circ, 15^\circ$	✓	×	$\pm 90^\circ, 180^\circ$	7,10	11.1	< 10	20°	0.8
[10]	31	58.5	8.2	82	1.6×1.96	6	-	×	×	-	-	-	-	-	0.001
[17]	31	8	5	-	1.43×3.64	10.12	-	✓	×	-	-	-	-	-	-
[18]	30	15	10	>90	3.15×1.49	11.2	30.3°, 30.3°	×	×	-	-	-	-	-	0.25
[34]	26	7.6	4.5	>95	0.78×0.39	0.83	-	✓	✓	Up to 75°	7.6	12	-	-	0.8
[35]	24	7	5	-	-	-	$159^\circ, 74^\circ$	✓	×	-	13	12.7	8	$12^\circ, 130^\circ$	1.63
[36]	38 54	5 3.8	6.9 7.4	93.5 82.7	0.77×0.76 $f_c = 38\ GHz$	0.76	-	-	×	-	-	12.2	-	-	0.508
[42]	28	6.42	7.4	>80	0.42×0.49	0.49	$60^\circ, 75^\circ$	×	×	-	-	-	-	-	0.676
[43]	28	20	9.9	>96	2.19×3.24	17	$57^\circ, 52^\circ$	×	×	-	-	-	-	-	0.428
Prop. Ant. Array	28	5	6.5	>90	0.63×0.66	1	$60^\circ, 60^\circ$	✓	✓	Up to $\pm 50^\circ$	1	15	< 16	$21^\circ, 60^\circ$	0.32

low energy efficiency (EE). Therefore, hybrid beamforming is one of the best solutions because it increases the SE and EE metrics simultaneously. Here, a hybrid beamforming system setup is prepared, based on using PS with two bits in the proposed 8-element array filtenna and a horn antenna as a UE. A codebook of the possible beamforming angles and their corresponding phase matrix related to a phase of PSs can be prepared. A processor can recall this codebook from its memory after receiving direction of arrival (DoA) and can make a decision about the bias of diodes across the desired angles. This matrix can be obtained by various optimal and sub-optimal methods [37], [38], [39]. The hybrid beamforming problem with phased uniform planar array (UPA) with limited bits of PS can be represented as follows

$$\begin{aligned} &\min_{\mathfrak{F}_{rf}, \mathfrak{F}_{bb}} \left\| s - \hat{s} \right\|_F^2 \\ &s.t. \quad \left\| \mathfrak{F}_{bb} \mathfrak{F}_{rf} \right\|^2 \leq 1 \\ &\qquad \left| \left[\mathfrak{F}_{rf} \right]_{i,j} \right|^2 = 1, \quad \forall i, j; \end{aligned} \tag{14}$$

where $\boldsymbol{s}$ is the training pilot samples which are transmitted from the UE (horn antenna), and $\hat{s}$ related to estimations of the transmitted signal. The phase of the $\left[\mathfrak{I}_{rf}\right]_{i,j}$ equal to hybrid analog and digital beamforming are displayed with $\mathfrak{I}_{rf}$ and $\angle \left[\mathfrak{I}_{rf}\right]_{i,j} = \frac{2\pi}{\lambda} d\ (m \sin\varphi_l \sin\theta_l + n \cos\theta_l)$. Moreover, the $\mathfrak{I}_{bb}$ matrices at the BS (proposed filtenna array). The minimization problem (14) can be reformed as presented in [40] due to the elimination of $\boldsymbol{s}$. Therefore, the final nonconvex problem can be rewritten as

$$\begin{aligned} &\min_{\mathfrak{I}_{rf}, \mathfrak{I}_{bb}} \left\| \mathfrak{I} - \mathfrak{F}_{bb} \mathfrak{F}_{rf} \boldsymbol{H} \right\|_F^2 \\ &s.t. \quad \left\| \mathfrak{F}_{bb} \mathfrak{F}_{rf} \right\|^2 \leq P_t \\ &\qquad \left| \left[\mathfrak{F}_{rf} \right]_{i,j} \right|^2 = 1, \quad \forall i, j; \end{aligned} \tag{15}$$

where $\boldsymbol{H} = \sqrt{\frac{N_t N_r}{N_l}} \sum_{l=1}^{N_l} \alpha_l \mathbf{a_r}(\varphi_l, \theta_l)\, \mathbf{a_t^H}(\varphi_l, \theta_l)$, and where α_l shows the complex gain with path loss of the l^{th} path between UE and the UPA which is provided by the proposed filtenna array with post processing (as investigated in Fig. 17). The angles of arrival and departure (AoAs/AoDs) variables are denoted by $\varphi_l \in [0, 2\pi]$ and $\theta_l \in [0, \pi]$ respectively of the l^{th} path. $\mathbf{a_r}(\varphi_l, \theta_l)$, and $\mathbf{a_t^H}(\varphi_l, \theta_l)$ are respectively indicated as the antenna array response matrices at the BS and UE,. Here, $\mathbf{a_t^H}(\varphi_l, \theta_l) = 1$, $\varphi_l = \pi/4$, and $\theta_l = \pi/6$. In this experiment, the line-of-sight (LoS) channel is the only one to be considered because it can be test in a chamber room and the signal-to-noise ratio (SNR) can be established using a noise generator PE85N1008. In this paper, a learning method is proposed to provide the correct PS angles for beamforming, which is defined as ADMM-BO in order to solve the beamforming problem in an iterative structure. The minimization problem is presented as an N_t sub-array problem as follows:

$$F(\phi) = \sum_{i=1}^{N_t} \boldsymbol{f}^i(\phi) \tag{16}$$

where $\phi = \frac{2\pi}{\lambda} d\ (m \sin\varphi_l \sin\theta_l + n \cos\theta_l)$ for UPA and $\boldsymbol{f}^i(\phi) = \left\| \boldsymbol{I}^i - \boldsymbol{f}_{bb}^i \mathfrak{F}_{rf}(\phi) \boldsymbol{H} \right\|_2^2$. Thereby, a multi-objective optimization problem (MOOP) can be defined over a finite angle space. To solve these sub-problem, two steps should be considered:

- A digital beamformer should be calculated with a fixed analog beamformer $\mathfrak{F}_{rf}(\phi)$, whichcan be solved by least

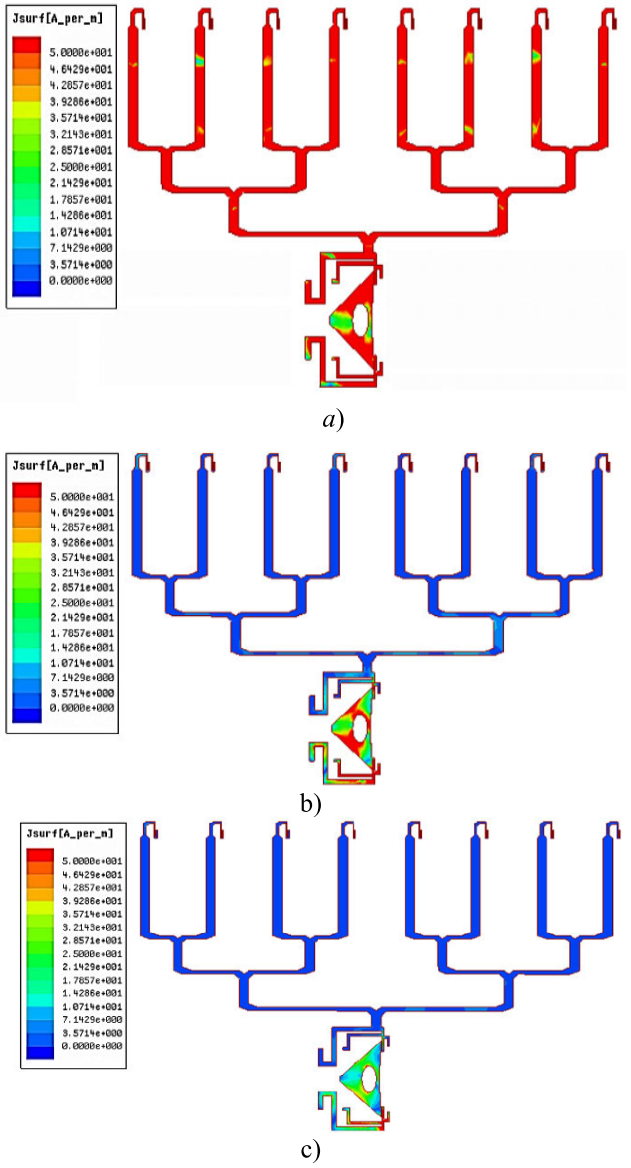

FIGURE 15. The surface current distribution of the proposed 5G array filtenna for in-band and out-of-band frequencies.: a) 28 GHz (in-band), b) 26 GHz (out-out-band), c) 30 GHz (out-out-band).

square (LS) solution $\boldsymbol{f}_{\boldsymbol{bb}}^{\boldsymbol{i}} = \left(\mathfrak{F}_{\boldsymbol{rf}}(\phi)\boldsymbol{H}\right)^{\mathrm{t}}$, where $(\cdot)^{\mathrm{t}}$ means the moore-penrose pseudo inverse, and $\boldsymbol{f}_{\boldsymbol{bb}}^{\boldsymbol{i}}$ means the i^{th}row of the digital beamformer matrix.

- An analog beamformer should be solved with respect to the power limit $\left\|\mathfrak{F}_{\boldsymbol{bb}}\mathfrak{F}_{\boldsymbol{rf}}\right\|^2 \leq 1$ and amplitude of PS $(\left|\mathfrak{F}_{\boldsymbol{rf}}\right|_{i,j} \in \{0, 1\})$.

In order to solve this MOOP, (17) should be reformulated in this form with $\boldsymbol{N_t}$ supplementary variables, which means one variable per constraint function in $\sum_{i=1}^{N_t} 1(I(\phi) > 0)$ as follows:

These two unknown objectives in the sub-problems can be solved with iterative ADMMBO learning method as follows:

$$\min_{\boldsymbol{\phi}, \boldsymbol{\Upsilon}_1, \ldots, \boldsymbol{\Upsilon}_{N_t}} \sum_{\boldsymbol{i=1}}^{N_t} \boldsymbol{f}^{\boldsymbol{i}}(\boldsymbol{\phi}) + \sum_{i=1}^{N_t} 1\left(I\left(\boldsymbol{\Upsilon_i}\right) > 0\right)$$

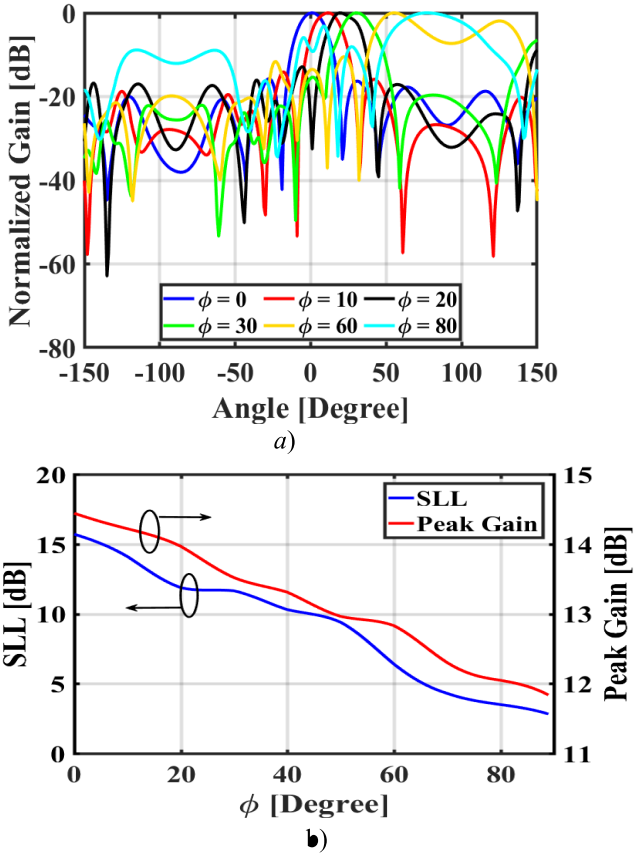

FIGURE 16. a) The normalized measured beam steering patterns of the proposed phased array filtenna for different angles, b) The measured SLL and peak gain of the beam-steering patterns of the proposed phased array filtenna for different angles.

$$s.t.\ \phi = \boldsymbol{\Upsilon_i}, i = 1, \ldots, N_t \tag{17}$$

where $\mathcal{J}(\phi) = \left\|\mathfrak{F}_{\boldsymbol{bb}}\mathfrak{F}_{\boldsymbol{rf}}\right\|^2$, $1(\mathcal{J}(\phi) > 0)$ shows the indicator function with one for $\mathcal{J}(\phi) > 0$ and otherwise becomes zero. Then an iterative ADMM structure for (17) at the k$^{\mathrm{th}}$ iteration is processed as shown below.

$$\begin{cases} \phi_{k+1} = \underset{\boldsymbol{\phi}}{\operatorname{argmin}} \boldsymbol{f^i}(\phi) + \frac{\rho}{2}\left\|\phi - \Upsilon_i^k + \frac{\boldsymbol{\omega_i^k}}{\boldsymbol{\rho}}\right\|_2^2 \\ \Upsilon_i^{k+1} = \underset{\boldsymbol{\phi}}{\operatorname{argmin}}\, 1\left(\mathcal{J}(\Upsilon_i) > 0\right) + \frac{\rho}{2}\left\|\phi_{k+1} - \Upsilon_i^k + \frac{\boldsymbol{\omega_i^k}}{\boldsymbol{\rho}}\right\|_2^2 \\ \omega_i^{k+1} = \omega_i^k + \rho\left(\phi_{k+1} - \Upsilon_i^{k+1}\right), \forall i = 1, \ldots, N_t \end{cases} \tag{18}$$

The unconstrained objective function is minimized with respect to $\boldsymbol{\phi}$ related, to impose the iterative solution that leads to a feasible region. The second one finds the feasible point of constraint which is used by the optimal sub-problem and indicates the feasibility sub-problem [41].

- ADMM iterative procedure.
- BO iterative procedure to solve two optimality and feasibility sub-problems
- Expected improvement $EI(\cdot)$ used to solve sub-problems.

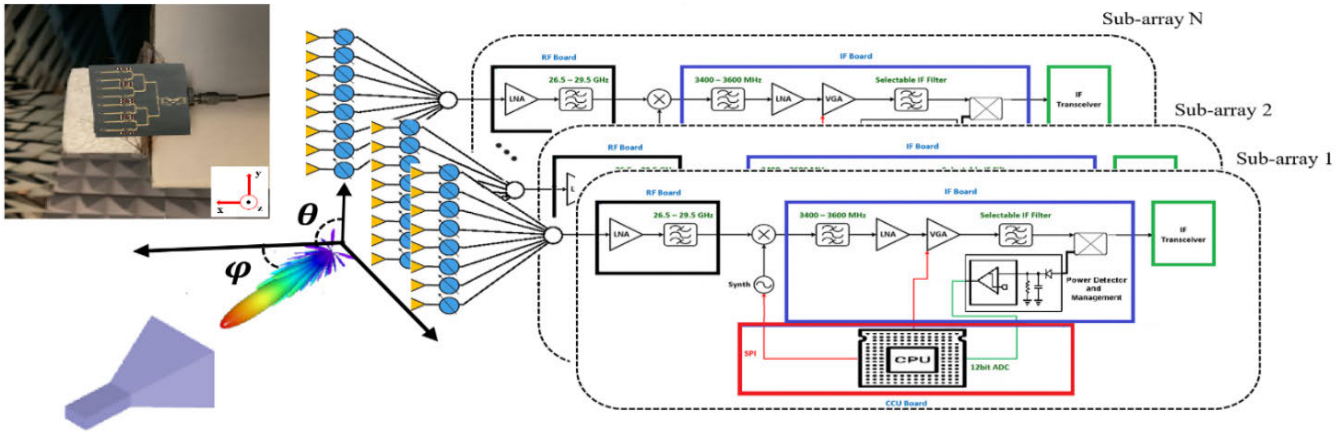

a)

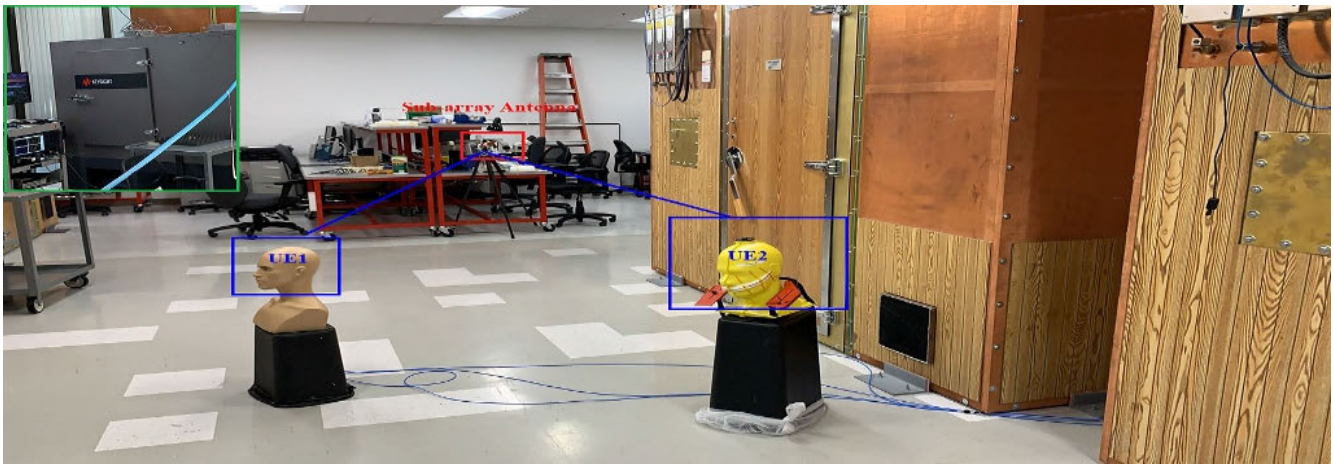

b)

FIGURE 17. A practical 5G mmWave system Setup which contains one UE and 32-element antenna array (4 × 8-elements): a) The LoS scenario (chamber room), b) The LoS scenario (real channel).

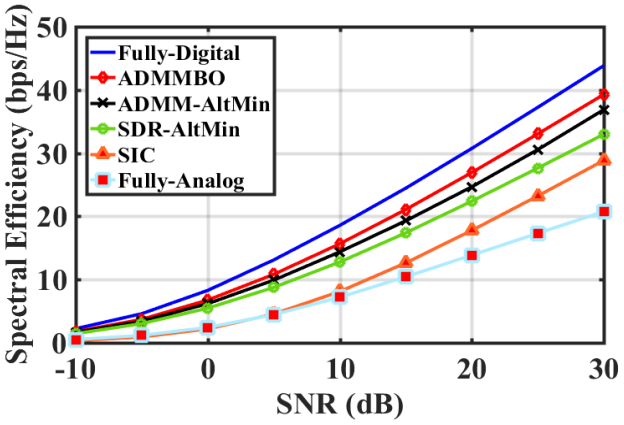

FIGURE 18. Spectral efficiency versus SNR for 5G mmWave channel achieved by different beamforming algorithms when $N_r = 16, N_{sub} = 4$ and $K = 4, N_t = 1$.

The main advantage of the $EI(\cdot)$ factor is its simplicity in comparison to the stochastic gradient descent optimization method. It can be applied at any angle. As presented in [41], $f^i(\phi)$ can be modeled in a Gaussian process (GP) as an unknown function, besides the second term $\frac{\rho}{2}\left\|\phi_l - \Upsilon_i^k + \frac{\omega_i^k}{\rho}\right\|_2^2$ is assumed to be a constant and known function due to the fixed amount of Υ_i^k, ω_i^k and any assumed ϕ. Therefore, $u(\phi)$ can be written as

$$u^k(\phi) = \boldsymbol{f^i}(\phi) + \frac{\rho}{2}\left\|\phi - \Upsilon_i^k + \frac{\boldsymbol{\omega_i^k}}{\boldsymbol{\rho}}\right\|_2^2 \tag{19}$$

For the given data $\mathcal{F} = \left\{(\phi_l, \boldsymbol{f^i}(\phi_l))\right\}_{l=1}^{\boldsymbol{n}}$, the new sample set data from (19) is collected as $\mathcal{U}^k$. The standard $EI(\phi)$ is achieved as follows:

$$EI(\phi) = E_{u^k|U^k}\left[\max\left(0, u^{k+} - u^k(\phi)\right)\right] \tag{20}$$

where u^{k+} shows the best objective amount of $u^k(\phi)$, and the GP model of $u^k(\phi)$ becomes $p\left[u^k(\phi)|\mathcal{U}^k\right]$. Fig. 17 shows the details of the experimental system setup with block diagram for 5G communications. It can be seen the 5G mmWave testbed in an anechoic chamber has analog and digital components. In this test, one UE (horn antenna) is assumed to consider the throughput experiments in the LOS mmWave

Algorithm 1 ADMMBO for Hybrid Beamforming

Input: $\rho, n, m, \Upsilon_i^1, \omega_i^1, N_t, K, N_j, N_q, \varepsilon; \forall i = 1, \ldots, N_t, \forall k = 1, \ldots, K$
Generate random sample sets $\{\phi_l \in (-\pi, \pi)\}_{l=1}^{n}, \{\Upsilon_{l,i} \in (-\pi, \pi)\}_{l=1}^{m_i}$
Initialize: $k = 1, \mathcal{F}^1 = \left\{\left(\phi_l, f^i(\phi_l)\right)\right\}_{l=1}^{n}, \mathfrak{I}^1 = \{(\Upsilon_{l,i}, \mathcal{J}(\Upsilon_{l,i}))\}_{l=1}^{m_i}, S = 0$
While $k \leq K$, S $= = 0$ **do**
  for $j = 1, \ldots, N_j$ **do**
    Compute $\mathcal{U}^j = \left\{\left(\phi_l, f^i(\phi_l) + \frac{\rho}{2}\left\|\phi_l - \Upsilon_i^1 + \frac{\omega_i^1}{\rho}\right\|_2^2\right)\right\}_{l=1}^{n}$
    GP posterior updating $p\left[u(\phi)|\mathcal{U}^j\right]$
    $\underset{\phi \in (-\pi, \pi)}{\text{argmax}}\ EI(\phi) \rightarrow \phi^j, \mathcal{F}^{j+1} = \mathcal{F}^j \cup \left\{\phi_l, f^i(\phi_l)\right\}$
    $n = n + 1$
  end for
  $\phi_{k+1} = \underset{\phi \in \mathcal{F}^{N_j}}{\text{argmax}} f^i(\phi) + \frac{\rho}{2}\left\|\phi - \Upsilon_i^1 + \frac{\omega_i^1}{\rho}\right\|_2^2$
  $\mathcal{F}^{k+1} = \mathcal{F}^{N_j}$
  for $i = 1, \ldots, N_t$ **do**
  for $q = 1, \ldots, N_q$ **do**
    Compute $V_i^q = \left\{\left(\Upsilon_{l,i}^k, \mathbf{1}\left(\mathcal{J}\left(\Upsilon_{l,i}^k\right) > 0\right) + \frac{\rho}{2}\left\|\phi_{k+1} - \Upsilon_{l,i}^k + \frac{\omega_i^k}{\rho}\right\|_2^2\right)\right\}_{l=1}^{m_i}$
    GP posterior updating $p\left[v(\Upsilon_i^k)|V_i^q\right]$
    $\underset{\phi \in (-\pi, \pi)}{\text{argmax}}\ EI(\phi) \rightarrow \Upsilon_i^{k,q}, \mathfrak{I}_i^{q+1} = \mathfrak{I}_i^q \cup \left\{\Upsilon_i^{k,q}, \mathcal{J}\left(\Upsilon_i^{k,q}\right)\right\}$
    $m_i = m_i + 1$
  end for
  $\Upsilon_i^{k+1} = \underset{\Upsilon_i^K \in \mathfrak{I}^{Nq}}{\text{argmax}} f^i(\phi) + \frac{\rho}{2}\left\|\phi_{k+1} - \Upsilon_i^k + \frac{\omega_i^k}{\rho}\right\|_2^2$
  $\mathfrak{I}_i^{k+1} = \mathfrak{I}^{Nq}$
  $\omega_i^{k+1} = \omega_i^k + \rho\left(\phi_{k+1} - \Upsilon_i^{k+1}\right)$
  $\delta_i^{k+1} = \phi_{k+1} - \Upsilon_i^{k+1}$
  $\Delta_i^{k+1} = -\rho\left(\phi_{k+1} - \Upsilon_i^{k+1}\right)$
  end for
  if $\left\|\delta_i^{k+1}\right\|_2 \leq \varepsilon$ and $\left\|\Delta_i^{k+1}\right\|_2 \leq \varepsilon$ **then**
  S $= 1$ **end if**
  k=k+1
end while
if S $= 1$ **then**
  $\phi_{opt} = \phi_{k+1}$
else
  $\phi_{opt} = \underset{\phi \in \mathcal{F}^K \cup \mathfrak{F}_1^K \cup \ldots \cup \mathfrak{F}_{N_t}^K}{\text{argmin}} E_{F|\mathcal{F}^K}[F(\phi)]$ s.t. $p\left[\mathcal{J}(\phi) < 0\right] \geq 1 - \varphi$
end if

channels. In this test, the partially-connected structure is configured with a 1×4 digital baseband beamformer matrix and a 4×8 analog RF beamformer matrix for an 8×1 mmWave channel on any side of the USPA. Data packets are received from an antenna with $N_r = 16, N_{sub} = 4$ with USPA equipped for $K = 4$ users with $N_t = 1$ antenna. The mmWave channel parameters are established as $N_{cl} = 4$ clusters, $N_{ray} = 3$ rays. First, the SE performance versus SNR is investigated with various algorithms when the number of RF chains is the same as the data streams shown in Fig. 18.

Here, the partially-connected structure is employed because the proposed 5G mmWave filter-antenna array for various beamforming algorithms is being tested. It can be seen the proposed ADMMBO learning method provides better performance gains over state-of-art methods as presented in [39], particularly at higher SNRs. This is generally because

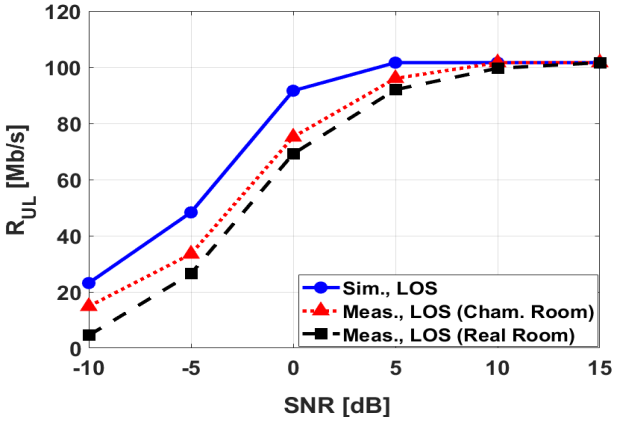

FIGURE 19. Simulation and measurement result of data-rate versus the SNR with QPSK for the LOS channel in both the proposed ADMM-BO hybrid beamforming and the phased filtenna array setup system.

this method searches for the nearest point by an effective search strategy to the optimum point that relates to the feasible answer set. Fig. 19 investigates the simulation and measurement result of the experimental 5G mmWave setup with respect to data-rate versus SNR with QPSK modulation for LOS channel at $\varphi_l = \pi/4$, $\theta_l = \pi/6$ in 28 GHz with 100 MHz BW. Specifically, the black solid line and the black dotted line show the appropriate and compatible performance of the proposed ADMM-BO hybrid beamforming which is tested by the suggested phased filtenna array in the PC structure form of a mmWave setup system.

VI. CONCLUSION

In this paper, a high gain double up-down U-shaped bend antenna and its array filtenna for the 5G communication systems with theoretical discussion is proposed. A double dipole is inserted at the ground plane to control the gain and focusing of the main beam. The results indicate that the proposed single 5G antenna has an IBW of around 7.14% and a gain of about 6.7 dBi at the frequency of 28 GHz. The proposed 5G filter has 4% IBW and lower than 0.6 dB attenuation on the passband. The filter has small dimensions and a thin substrate. Moreover, a simple 2-bit structure involving an mmWave phase-shifter is designed with a shift phase around 90°, 180°, and 270° in order to have beam-steering. Finally, a linear phase array filtenna is proposed using 8 elements of the single 5G with 0.35λ spacing between any two elements and using a stub-line to reduce the mutual coupling and the 5G- mmWave filter before the first power divider. The phased array filtenna is fabricated for use in the 5G array beamforming. The measured results show the IBW at approximately 3.5% with a high gain of 15 dBi. The proposed 5G phased array filtenna can scan the main beam in the range of [-50°, 50°] with variations in gain of around 1.5 dB and a minimum SLL of about -10 dB at angle 50°. Finally, a novel hybrid beamforming is proposed, named the ADMM-BO learning method, in order to increase the SE and the data-rate which is experimentally tested with the suggested phase filtenna array.

ACKNOWLEDGMENT

The authors would like to express their great appreciation to Dr. Sajjad Abazari Aghdam for his valuable and constructive suggestions during the development of this research work.

REFERENCES

[1] H. A. Diawuo and Y. Jung, "Broadband proximity-coupled microstrip planar antenna array for 5G cellular applications," *IEEE Antennas Wireless Propag. Lett.*, vol. 17, no. 7, pp. 1286–1290, Jul. 2018.

[2] M. Nouri, H. Behroozi, A. Jafarieh, S. A. Aghdam, M. J. Piran, and N. K. Mallat, "A learning-based dipole Yagi–Uda antenna and phased array antenna for mmWave precoding and V2V communication in 5G systems," *IEEE Trans. Veh. Technol.*, vol. 72, no. 3, pp. 2789–2803, Mar. 2022.

[3] D. Parker and D. C. Zimmermann, "Phased arrays—Part 1: Theory and architectures," *IEEE Trans. Microw. Theory Techn.*, vol. 50, no. 3, pp. 678–687, Mar. 2002.

[4] D. Parker and D. C. Zimmermann, "Phased arrays—Part II: Implementations, applications, and future trends," *IEEE Trans. Microw. Theory Techn.*, vol. 50, no. 3, pp. 688–698, Mar. 2002.

[5] N. K. Mallat, M. Nouri, S. A. Aghdam, M. T. Zia, B. Harb, and A. Jafarieh, "A dual circularly reconfigurable polarization patch antenna for fifth generation mobile communication systems," *Prog. Electromagn. Res. C*, vol. 105, pp. 73–84, 2020.

[6] I. Syrytsin, S. Zhang, G. F. Pedersen, and A. S. Morris, "Compact quad-mode planar phased array with wideband for 5G mobile terminals," *IEEE Trans. Antennas Propag.*, vol. 66, no. 9, pp. 4648–4657, Sep. 2018.

[7] M. Nouri, S. A. Aghdam, A. Jafarieh, J. Bagby, and S. Sahebghalam, "A wideband millimeter-wave antenna based on quasi-Yagi antenna with MIMO circular array antenna beamforming for 5G wireless networks," *Microw Opt Technol Lett.*, vol. 61, no. 7, pp. 1–5, 2019.

[8] H. Kim, B. Park, S. Song, T. Moon, S. Kim, J. Kim, J. Chang, and Y. Ho, "A 28-GHz CMOS direct conversion transceiver with packaged 2 × 4 antenna array for 5G cellular system," *IEEE J. Solid-State Circuits*, vol. 53, no. 5, pp. 1245–1259, May 2018.

[9] T. K. Vo Dai, T. Nguyen, and O. Kilic, "Compact multi-layer microstrip Rotman lens design using coupling slots to support millimetre wave devices," *IET Microw., Antennas Propag.*, vol. 12, no. 8, pp. 1260–1265, Jul. 2018.

[10] S. F. Jilani, Q. H. Abbasi, and A. Alomainy, "Inkjet-printed millimetre-wave PET-based flexible antenna for 5G wireless applications," in *IEEE MTT-S Int. Microw. Symp. Dig.*, Aug. 2018, pp. 1–3.

[11] W. Lin, R. W. Ziolkowski, and T. C. Baum, "28 GHz compact omnidirectional circularly polarized antenna for device-to-device communications in the future 5G systems," *IEEE Trans. Antennas Propag.*, vol. 65, no. 12, pp. 6904–6914, Dec. 2017.

[12] H. Shaman, S. Almorqi, O. Haraz, S. Alshebeili, and A. Sebak, "Millimeter-wave microstrip diplexer using elliptical open-loop ring resonators for next generation 5G wireless applications," in *Proc. Medit. Microw. Symp. (MMS)*, Dec. 2014, pp. 1–4.

[13] A. Iqbal, J. J. Tiang, C. K. Lee, N. K. Mallat, and S. W. Wong, "Dual-band half mode substrate integrated waveguide filter with independently tunable bands," *IEEE Trans. Circuits Syst. II, Exp. Briefs*, vol. 67, no. 2, pp. 285–289, Feb. 2020.

[14] R. Bowrothu, Y. Yoon, and J. Zhang, "Through glass via (TGV) based band pass filter for 5G communications," in *Proc. IEEE 68th Electron. Compon. Technol. Conf. (ECTC)*, San Diego, CA, USA, May 2018, pp. 1097–1102.

[15] A. Iqbal, A. W. Ahmad, A. Smida, and N. K. Mallat, "Tunable SIW bandpass filters with improved upper stopband performance," *IEEE Trans. Circuits Syst. II, Exp. Briefs*, vol. 67, no. 7, pp. 1–5, Aug. 2019.

[16] M. Nouri, A. Jafarieh, H. Behroozi, N. K. Mallat, M. H. Jamaluddin, and S. A. Aghdam, "Compact 5G millimeter-wave dual-band filter with application in filtenna," *Microw. Opt. Technol. Lett.*, vol. 62, pp. 1–5, Feb. 2020.

[17] I. Syrytsin, M. Shen, and G. F. Pedersen, "Antenna integrated with a microstrip filter for 5G mm-Wave applications," in *Proc. Int. Conf. Electromagn. Adv. Appl. (ICEAA)*, Sep. 2018, pp. 438–441.

[18] K. Yang, M. Hoang, X. Bao, P. McEvoy, and M. J. Ammann, "Dual-stub Ka-band Vivaldi antenna with integrated bandpass filter," *IET Microw., Antennas Propag.*, vol. 12, no. 5, pp. 668–671, Apr. 2018.

[19] A. F. Molisch, M. Z. Win, and J. H. Winters, "Reduced-complexity transmit/receive-diversity systems," *IEEE Trans. Signal Process.*, vol. 51, no. 11, pp. 2729–2738, Nov. 2003.

[20] P. Sudarshan, N. Mehta, A. Molisch, and J. Zhang, "Channel statistics-based RF pre-processing with antenna selection," *IEEE Trans. Wireless Commun.*, vol. 5, no. 12, pp. 3501–3511, Dec. 2006.

[21] X. Zhang, A. F. Molisch, and S.-Y. Kung, "Variable-phase-shift-based RF-baseband codesign for MIMO antenna selection," *IEEE Trans. Signal Process.*, vol. 53, no. 11, pp. 4091–4103, Nov. 2005.

[22] R. W. Heath, N. Gonzalez-Prelcic, S. Rangan, W. Roh, and A. M. Sayeed, "An overview of signal processing techniques for millimeter wave MIMO systems," *IEEE J. Sel. Topics Signal Process.*, vol. 10, no. 3, pp. 436–453, Apr. 2016.

[23] S. Han, I. Chih-Lin, Z. Xu, and C. Rowell, "Large-scale antenna systems with hybrid analog and digital beamforming for millimeter wave 5G," *IEEE Commun. Mag.*, vol. 53, no. 1, pp. 186–194, Jan. 2015.

[24] X. Yu, J. Zhang, and K. B. Letaief, "A hardware-efficient analog network structure for hybrid precoding in millimeter wave systems," *IEEE J. Sel. Topics Signal Process.*, vol. 12, no. 2, pp. 282–297, May 2018.

[25] *Ansys HFSS*. (Oct. 2022). [Online] Available: www.ansys.com/Products/Electronics/ANSYS-HFSS

[26] D. M. Pozar, "Transmission line theory," *Microwave Engineering*, 4th ed. Hoboken, NJ, USA: Wiley, 2011, pp. 48–94.

[27] D. K. Cheng, *Field and Wave Electromagnetics*. Tamil Nadu, India: Pearson Education India, 1989.

[28] B. K. Kanaujia, M. K. Khandelwal, S. Dwari, S. Kumar, and A. K. Gautam, "Analysis and design of compact high gain microstrip patch antenna with defected ground structure for wireless applications," *Wireless Pers. Commun.*, vol. 91, no. 2, pp. 661–678, Nov. 2016.

[29] H. H. M. Ghouz, M. F. A. Sree, and M. A. Ibrahim, "Novel wideband microstrip monopole antenna designs for WiFi/LTE/WiMax devices," *IEEE Access*, vol. 8, pp. 9532–9539, 2020.

[30] M. Tang, Q. Lin, M. Li, and R. W. Ziolkowski, "Polarization-reconfigurable Yagi-configured electrically small antenna," *IEEE Trans. Antennas Propag.*, vol. 69, no. 3, pp. 1757–1762, Mar. 2021, doi: 10.1109/TAP.2020.3018554.

[31] Y.-L. Kuo and K.-L. Wong, "Printed double-T monopole antenna for 2.4/5.2 GHz dual-band WLAN operations," *IEEE Trans. Antennas Propag.*, vol. 51, no. 9, pp. 2187–2192, Sep. 2003.

[32] J. Tao, Q. Feng, G. A. E. Vandenbosch, and V. Volskiy, "Director-loaded magneto-electric dipole antenna with wideband flat gain," *IEEE Trans. Antennas Propag.*, vol. 67, no. 11, pp. 6761–6769, Nov. 2019.

[33] Z. Yang, L. Zhang, and T. Yang, "A microstrip magnetic dipole Yagi–Uda antenna employing vertical I-shaped resonators as parasitic elements," *IEEE Trans. Antennas Propag.*, vol. 66, no. 8, pp. 3910–3917, Aug. 2018.

[34] G. Hua, C. Yang, P. Lu, H.-X. Zhou, and W. Hong, "Microstrip folded dipole antenna for 35 GHz MMW communication," *Int. J. Antennas Propag.*, vol. 2013, pp. 1–6, Nov. 2013.

[35] N. O. Parchin, M. Alibakhshikenari, H. J. Basherlou, R. A. Abd-Alhameed, J. Rodriguez, and E. Limiti, "mm-Wave phased array quasi-Yagi antenna for the upcoming 5G cellular communications," *Appl. Sci.*, vol. 9, no. 5, p. 978, Mar. 2019.

[36] C. Yu, E. S. Li, H. Jin, Y. Cao, G. Su, W. Che, and K. Chin, "24 GHz horizontally polarized automotive antenna arrays with wide fan beam and high gain," *IEEE Trans. Antennas Propag.*, vol. 67, no. 2, pp. 892–904, Feb. 2019.

[37] J.-C. Chen, "Hybrid beamforming with discrete phase shifters for millimeter-wave massive MIMO systems," *IEEE Trans. Veh. Technol.*, vol. 66, no. 8, pp. 7604–7608, Aug. 2017.

[38] A. A. Nasir, H. D. Tuan, T. Q. Duong, H. V. Poor, and L. Hanzo, "Hybrid beamforming for multi-user millimeter-wave networks," *IEEE Trans. Veh. Technol.*, vol. 69, no. 3, pp. 2943–2956, Mar. 2020.

[39] C. Fang, B. Makki, J. Li, and T. Svensson, "Hybrid precoding in cooperative millimeter wave networks," *IEEE Trans. Wireless Commun.*, vol. 20, no. 8, pp. 5373–5388, Aug. 2021.

[40] A. Vizziello, P. Savazzi, and K. R. Chowdhury, "A Kalman based hybrid precoding for multi-user millimeter wave MIMO systems," *IEEE Access*, vol. 6, pp. 55712–55722, 2018.

[41] S. Ariafar, J. Coll-Font, D. Brooks, and J. Dy, "ADMMBO: Bayesian optimization with unknown constraints using ADMM," *J. Mach. Learn. Res.*, vol. 20, no. 123, pp. 1–26, 2019.

[42] M. Nouri, S. A. Aghdam, A. Jafarieh, N. K. Mallat, M. H. Jamaluddin, and M. Dor-Emami, "An optimized small compact rectangular antenna with meta-material based on fast multi-objective optimization for 5G mobile communication," *J. Comput. Electron.*, vol. 20, no. 4, pp. 1532–1540, Aug. 2021.

[43] A. Jafarieh, M. Nouri, and H. Behroozi, "Optimized 5G-MMW compact Yagi–Uda antenna based on machine learning methodology," in *Proc. 29th Iranian Conf. Electr. Eng. (ICEE)*, May 2021, pp. 751–756, doi: 10.1109/ICEE52715.2021.9544194.

MAHDI NOURI (Member, IEEE) received the B.S. degree in telecommunication engineering from the University of Tabriz, Tabriz, in 2009, and the M.Sc. degree in telecommunication engineering from the Iran University of Science and Technology (IUST), Tehran, Iran, in 2012. From 2017 to 2019, he was an Assistant Professor (Lecturer) with the Department of Electrical Engineering, Electronics and Telecommunications, Arak University of Technology, Arak, Iran. He is currently a Research Fellow with the Sharif University of Technology (SUT) and the Senior Project Manager of 5G Communication Systems with Mobile Telecommunication Company of Iran (MCI) who is the first and largest mobile operators in Middle-East. He is also an Iran State-Member and a Sector-Member of MCI in the International Telecommunication Union (ITU). He has published more than 40 journal and conference papers. He was successfully selected for the Iran Postdoctoral Innovative Talent Support Program from the Iran National Science Foundation (INSF), Sharif University of Technology (SUT). His research interests include physical layer of 6G communication systems and B5G communication systems, deep reinforcement learning, machine learning in mobile communication systems, NFV-MANO for management, and orchestration of cloud networks. He is the winner of the 2017 Young Scientists Award from Iran's National Elites Foundation (INEF) and the Outstanding Doctoral Society Award of the University of Isfahan. He served on the editorial boards of the IEEE TRANSACTION journals and conferences.

ALIREZA JAFARIEH (Student Member, IEEE) received the B.Sc. degree in electrical engineering from the Arak University of Technology, Iran, 2019. He is currently pursuing the M.Sc. degree in field and waves with the Sharif University of Technology, Iran. His research interests include wireless telecommunication systems as 5G and 6G mobile systems.

HAMID BEHROOZI (Member, IEEE) received the B.Sc. degree in electrical engineering from the University of Tehran, Tehran, Iran, in 2000, the M.Sc. degree in electrical engineering from the Sharif University of Technology, Tehran, in 2003, and the Ph.D. degree in electrical engineering from Concordia University, Montreal, QC, Canada, in 2007. He is currently an Associate Professor with the Department of Electrical Engineering, Sharif University of Technology. He has authored over 40 journal articles and holds two patents. His research interests include information theory, joint source-channel coding, artificial intelligence in signal processing and data science, and cooperative communications.

NAZIH KHADDAJ MALLAT (Senior Member, IEEE) received the bachelor's degree in electrical and electronics engineering from Lebanese University, Lebanon, in 2000, the master's degree in IT from IMT Atlantique, France, in 2002, and the Ph.D. degree in telecommunications from the University of Quebec, Canada, in 2010. After his Ph.D. and until January 2012, he was a Postdoctoral Fellow with Ecole Polytechnique de Montreal. In 2013, he joined the College of Engineering, Al Ain University (AAU), United Arab Emirates, as an Assistant Professor, and was promoted to an Associate Professor, in 2019, where he was the Head of the Networks and Communication Engineering and Computer Engineering Department, from 2013 to 2017, the Deputy Dean of the College of Engineering, from 2014 to 2015, the Dean of the College of Engineering, from 2015 to 2018, the Director of the Quality Assurance and Institutional Research Center, from 2018 to 2020. Since November 2020, he has been the Vice President of Accreditation and Quality Assurance. He has acquired extensive teaching experience at both undergraduate and graduate levels. He has effectively taught many courses, and their relevant practical elements in laboratories at multiple Montreal universities (ETS, TELUQ, and Ecole Polytechnique de Montreal). His main research interests include passive microwave/millimeter-wave circuit, antennas, and filters, where he authored or coauthored over 60 publications. He is a member of Ordre des Ingénieurs du Québec, Canada, and Order of Engineers and Architects Tripoli, Lebanon. The "Fonds Québécois de la Recherche sur la Nature et les Technologies-FQRNT," a granting agency of the Quebec Government, has awarded him two prestigious scholarships for his doctoral studies, in 2008, a Postdoctoral Research, from 2010 to 2011, and thanks to his highest level of achievement. He is also the Founder of the IEEE AAU Student Branch and the IEEE UAE MTT-S Chapter (and later the IEEE UAE MTT-S & IM-S & AP-S Joint Chapter). He was the Vice-Chair of the IEEE Montreal Section 2007–2008, Membership Development Chair, from 2009 to 2010, and the Section Chair from 2011 to 2012. He has served in the steering committee of many IEEE international conferences. He was the IEEE UAE Technical Activities Coordinator, from 2015 to 2018, the IEEE Region 8 Chapter Coordination Subcommittee Chair, in 2015 and 2016, and the Organizing Committee Chair of three major events hosted by Al Ain University: 1st IEEE International Workshop at AAU, in February 2014, 11th IEEE UAE Student Day, in May 2016, and 16th Mediterranean Microwave Symposium (MMS2016), in November 2016.

AMJAD IQBAL (Member, IEEE) received the B.S. degree in electrical engineering from COMSATS University, Islamabad, Pakistan, in 2016, the M.S. degree in electrical engineering from the CECOS University of IT and Emerging Science, Peshawar, Pakistan, in 2018, and the Ph.D. degree in engineering from Multimedia University, Cyberjaya, Malaysia, in 2021. He was a Labortary Engineer with the Department of Electrical Engineering, CECOS University Peshawar, from 2016 to 2018. His research interests include printed antennas, flexible antennas, implantable antennas, multiple-input and multiple-output (MIMO) antennas, dielectric resonator antennas, wireless power transfer, and synthesis of microwave components.

MD. JALIL PIRAN (Senior Member, IEEE) received the Ph.D. degree in electronics and information engineering from Kyung Hee University, South Korea, in 2016. He then continued his research career as a Postdoctoral Fellow with the Networking Laboratory, Kyung Hee University. He is currently an Assistant Professor with the Department of Computer Science and Engineering, Sejong University, Seoul, South Korea. He published a substantial number of technical papers in well-known international journals and conferences in the field of intelligent information and communication technology (IICT), specifically in the fields of machine learning, data science, wireless communications and networking, 5G/6G, the Internet of Things (IoT), and cyber security. There are several top journals in which he is an Editor, including IEEE TRANSACTIONS ON INTELLIGENT TRANSPORTATION SYSTEMS, *Journal of Engineering Applications of Artificial Intelligence* (Elsevier), *Journal of Physical Communication* (Elsevier), and *Journal of Computer Communication* (Elsevier). He was the Chair of the "5G and Beyond Communications" Session with the 2022 IEEE International Conference on Communications (ICC), and a Technical Committee Member of Several Conferences. In the worldwide community, he is an Active Delegate from South Korea to the Moving Picture Experts Group (MPEG). IAAM "Scientist Medal of the Year 2017" was awarded to him for notable and outstanding research in new age technology and innovation, in Stockholm, Sweden. In 2017, he was recognized by the Iranian Ministry of Science, Technology, and Research as an "Outstanding Emerging Researcher." In addition, his Ph.D. dissertation has been selected as the "Dissertation of the Year 2016" by the Iranian Academic Center for Education, Culture, and Research in the Engineering Group.

DUEHEE LEE (Member, IEEE) received the B.S. degree in electronic and electrical engineering from the Pohang University of Science and Technology, Pohang, South Korea, in 2004, and the M.S. and Ph.D. degrees in electrical and computer engineering from The University of Texas at Austin, Austin, TX, USA, in 2009 and 2015, respectively. He is currently an Assistant Professor with the Department of Electrical Engineering, Konkuk University, Seoul, South Korea.